

THE PRODUCTION OF AN ACTIVATED CARBON FROM A COKE PRECURSOR

Submitted by

NICOLAAS MALAN ROSSOUW

For the degree of MTech (Chemical Engineering)

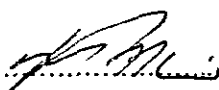
at the Cape Technikon

Supervisors: Prof F W Petersen
Dr F Prinsloo

Date: February 2002

DECLARATION

I hereby declare that the work contained in this thesis is my own work, except for where there is acknowledgement given in the text.



.....

MALAN ROSSOUW

FEBRUARY 2002

ABSTRACT

The activation of green “Smartie” coke (a mixture of medium temperature pitch and waxy oil coke) was investigated in a laboratory scale fluidised bed (FB) and a rotary kiln as function of (1) heat treatment temperature (HTT) and (2) heat treatment time (HTt). Activation in the FB was more effective (in terms of surface area development) and the product obtained from this type of reactor had a larger percentage of mesopores than the products from the rotary kiln. It was possible to produce a product with an iodine number equal to 745 mg iodine per gram carbon.

The study revealed that it is possible to tune the pore structure of “Smartie” coke derived activated carbons by changing the activation device and systematically changing the activation conditions. It was possible to obtain products ranging from a predominantly microporous structure to products with a predominantly mesoporous structure. Unfortunately, in comparison to commercially available activated carbons, the total surface areas were still too low and it will be necessary to perform further investigations focussed on increasing the total surface areas.

The gold adsorption tests performed on the activated carbon compared well to those of activated carbon currently in use in the gold industry.

ACKNOWLEDGEMENTS

The author would like to express his gratitude to:

- ❖ Sasol Technology Research and Development whose financial support made this research possible
- ❖ The personnel of the Fundamental Carbon Research laboratory at Sasol Technology R & D for their help with the experimental set-up
- ❖ The management team of gasification that gave me time off work to do this research and my colleagues that had to work additional overtime in order for me to take time off
- ❖ My mentor Prof Francis Petersen for all the advice and help on the gold adsorption part of this research
- ❖ My co-mentor Dr Frans Prinsloo without whose help, guidance and suggestions this research would have been a whole lot more difficult
- ❖ God who deserves all honour and glory

TABLE OF CONTENTS

	Page
DECLARATION	ii
ABSTRACT	iii
ACKNOWLEDGEMENTS	iv
TABLE OF CONTENTS	v
LIST OF FIGURES	viii
LIST OF TABLES	xi
NOMENCLATURE	xiii
Chapter 1	
Research Orientation	
1.1 History of Activated Carbon	1
1.2 Definition of Activated Carbon	1
1.3 Main Applications of Activated Carbon	2
1.4 Manufacture of Activated Carbon	3
1.4.1 Carbonisation	4
1.4.2 Activation	4
1.4.2.1 Chemical Activation	4
1.4.2.2 Physical Activation	4
1.5 Contribution of this study	5
1.6 Objectives of the study	6
Chapter 2	
Theoretical Foundation for Characterisation Techniques	
2 Characterisation of activated carbon	
2.1 Introduction	7
2.2 Structure of activated carbon	7

TABLE OF CONTENTS

2.3 N ₂ adsorption isotherms	7
2.4 Pore size distribution	9
2.4.1 The Langmuir Theory	10
2.4.2 The BET Theory	10
2.5 Estimation of the micropore volume	
2.5.1 Dubinin-Raduskevich equation	11
2.5.2 Dubinin-Astakhof equation	12
2.5.3 Density functional theory (DFT)	13
2.5.4 T-Plot	14
2.6 Gold adsorption	
2.6.1 Introduction	14
2.6.2 Mechanism of gold adsorption	14
2.6.3 Factors influencing gold adsorption on activated carbon	15
2.6.3.1 Effect of pore size distribution on gold adsorption	16
2.6.3.2 Effect of oxygen and surface oxygen functional groups	16
2.6.3.3 Effect of other anions and cations in solution	16
2.6.3.4 Effect of pH	17
2.6.4 Kinetics of gold cyanide adsorption	17
2.7 Summary of characterisation methods used in this study	18
Chapter 3	
Experimental	
3.1 Reagents	19
3.2 Physical activation	19
3.3 Characterisation	23
3.4 BET and pore size distribution measurement	24
3.5 Gold adsorption tests	24
3.6 Water purification tests	25

TABLE OF CONTENTS

Chapter 4	
Optimisation of process parameters	
4.1 Proximate and ICP analysis	26
4.2 Iodine numbers and carbon conversion	26
Chapter 5	
Carbon characterisation	
Adsorption in "Smartie" coke derived activated carbon	41
Chapter 6	
Carbon adsorption tests	
6 Adsorption of gold cyanide onto activated carbon	52
6.1 Calculation of the rate constant	52
6.2 Influence of operating parameters	54
6.2.1 Effect of pH on gold adsorption	54
6.2.2 Effect of concentration on gold adsorption	54
6.2.3 Effect of mass of carbon used on adsorption of gold	55
6.2.4 Effect of environment of adsorption	55
6.3 Comparative study	58
6.4 Water purification	58
Chapter 7	
Concluding Remarks and Recommendations	
7.1 Conclusions	61
7.1.1 Method of characterisation	61
7.1.2 Gold adsorption	62
7.1.3 Water purification	62
7.2 Recommendations	62
References	64

LIST OF FIGURES

	Page
Chapter 2	
Theoretical Foundation for Characterisation Techniques	
Figure 2.1: The six basic adsorption isotherm types	8
Chapter 3	
Experimental	
Figure 3.1: Schematic drawing of rig for activation in laboratory rotary kiln	19
Figure 3.2: Experimental rig for activation in a rotary kiln	20
Figure 3.3: Schematic drawing of rig for activation in FB	21
Figure 3.4: Experimental rig for activation in a fluidised bed reactor	22
Figure 3.5: Schematic drawing of gold adsorption tests. A. Perspex reactor (side view), B Top view, C flat blade impeller	25
Chapter 4	
Optimisation of Process Parameters	
Figure 4.1: Iodine number versus heat treatment time	27
Figure 4.2: Response surface of time and temperature. a. Rotary kiln. b. FB	37
Figure 4.3: Reactivity as function of carbon conversion	40
Figure 4.4: Carbon conversion as function of time	40
Chapter 5	
Carbon characterisation	
Figure 5.1: Adsorption-isotherm of N ₂ by "Smartie" coke derived activated carbon a. activation in the rotary kiln (experimental conditions: steam LHSV = 5.68 cm ³ g h ⁻¹ ; T = 973 K; HTt = 7 hours b. activation in the FB (experimental conditions: steam LHSV = 61.7 cm ³ g h ⁻¹ ; T = 973 K)	42

LIST OF FIGURES

- Figure 5.2: Adsorption-isotherm of N_2 by "Smartie" coke derived activated carbon a. activation in the rotary kiln (experimental conditions : steam LHSV = $6.56 \text{ cm}^3 \text{ g h}^{-1}$ T = 1123 K) b. activation in the FB (experimental conditions : steam LHSV = $71.0 \text{ cm}^3 \text{ g h}^{-1}$; = 1123 K) **43**
- Figure 5.3: Adsorption-isotherm of N_2 by "Smartie" coke derived activated carbon a. activation in the rotary kiln (experimental conditions : steam LHSV = $6.85 \text{ cm}^3 \text{ g h}^{-1}$; T = 1173 K; HTt = 7 hours) b. activation in the FB (experimental conditions : steam LHSV = $74.3 \text{ cm}^3 \text{ g h}^{-1}$; T = 1173 K; HTt = 4 hours) **44**
- Figure 5.4: Micropore and micropore + mesopore volume per unit weight starting material as function of HTT a. activation in FB b. activation in rotary kiln. **46**
- Figure 5.5: Micropore volume per unit weight starting material as function of HTt **47**
- Figure 5.6: Pore size distribution of the activated carbon produced in the FB Experimental conditions: T = 973 K; LHSV = $61.7 \text{ cm}^3 \text{ g h}^{-1}$ **48**
- Figure 5.7: Pore size distribution of the activated carbon produced in the FB Experimental conditions: T = 1123 K; LHSV = $71.0 \text{ cm}^3 \text{ g h}^{-1}$ **49**
- Figure 5.8: Pore size distribution of the activated carbon produced in the rotary kiln Experimental conditions: T = 1123 K; LHSV = $6.56 \text{ cm}^3 \text{ g h}^{-1}$ **49**
- Figure 5.9: Pore size distribution of the activated carbon produced in the FB HTt = 7 Hours **50**
- Figure 5.10: Pore size distribution of the activated carbon produced in the rotary kiln: HTt = 7 hours **50**
- ### Chapter 6
- #### Carbon adsorption tests
- Figure 6.1: Adsorption tests at varying pH levels. $[Au_0] \sim 20 \text{ ppm}$, M = 0.2 g, N = 200 rpm **56**
- Figure 6.2: Adsorption tests at varying concentration levels. pH ~ 10 , M = 0.2 g, N = 200 rpm **56**

LIST OF FIGURES

- Figure 6.3: Adsorption tests at varying mass of activated carbon used pH ~ 10, [Au₀] ~ 20ppm, N = 200 rpm 57
- Figure 6.4: Calculated rate constant for adsorption with adsorption environment varied. pH ~ 10, [Au₀] ~ 20 ppm, M = 0.2 g, N = 200 rpm 57
- Figure 6.5: Comparison between gold adsorption of Smartie coke and ANK pH ~ 10, [Au₀] ~ 20 ppm, M = 0.2 g, N = 200 rpm 58
- Figure 6.6: DOC Results of the two test carbons 59

LIST OF TABLES

	Page
Chapter 1	
Research Orientation	
Table 1.1: Main applications of activated carbon	2
Table 1.2: Specifications for activated carbon to be used in the gold recovery industry	3
Table 1.3: Raw materials used for activated carbon in order of importance (tons / year)	3
Chapter 2	
Theoretical Foundation for Characterisation Techniques	
Table 2.1: Summary of characterisation methods used	18
Chapter 3	
Experimental	
Table 3.1: Kinetic models for char gasification reaction	21
Chapter 4	
Optimisation of Process Parameters	
Table 4.1: Characterisation of the "Smartie" coke	26
Table 4.2: Characteristics of Sasol activated carbons	28
Table 4.3: Requirements of commercially activated carbons used	35
Table 4.4: Proposed additional activation trials for the FB reactor	38
Chapter 6	
Carbon adsorption tests	
Table 6.1: Calculated rate constant for adsorption with pH varied. [Au ₀] ~ 20 ppm	53

LIST OF TABLES

Table 6.2:	Calculated rate constant for adsorption with $[Au_0]$ varied. pH ~ 10	53
Table 6.3:	Calculated rate constant for adsorption with mass of activated carbon used varied: pH ~ 10, $[Au_0]$ ~ 20 ppm	53
Table 6.4:	Calculated rate constant for adsorption with adsorption environment varied. pH ~ 10, $[Au_0]$ ~ 20 ppm	54
Table 6.5:	Characteristics of the test carbons for water purification	60

NOMENCLATURE

A	adsorption potential in DR-equation
C	cm ³ of Na ₂ S ₂ O ₃ used
D	density conversion factor (cm ³ liquid / cm ³ STP)
E	energy parameter (kJ mol ⁻¹)
E ₀	surface characteristic energy (kJ mol ⁻¹)
g	mass of sample used in grams
HTT	heat treatment temperature (K)
HTt	heat treatment time (h)
M	molecular mass of adsorbent
n	structural heterogeneity parameter
N ₀	mass before activation
N ₁	normality of iodine solution
N ₂	normality of Na ₂ S ₂ O ₃ solution
N _a	Avogadro's number
P/P ₀	relative pressure
r	gasification rate
SA	BET surface area (m ² g ⁻¹)
T	temperature (K)
t	time (h)
V _a	standard volume
V _{ads}	quantity adsorbed at relative pressure
V ₀	liquid micropore volume
V _m	monolayer coverage
W _{ash}	mass at 100% carbon conversion
W ₀	mass before activation
W _t	mass after activation
X	carbon conversion

NOMENCLATURE

- X/M milligram of iodine adsorbed per gram of carbon
- α area covered by one molecule of N_2
- ρ density of the adsorbed phase
- ξ constant in the DR equation
- $\rho(r)$ equilibrium density at a general 3-space co-ordinate r in the DFT calculations
- μ chemical potential in the DFT calculations
- $[Au]$ gold concentration in the bulk solution (mg / dm³)
- $[Au_c]$ gold concentration on the carbon surface (mg / dm³)
- $[Au_0]$ initial gold concentration in the solution (mg / dm³)
- k_f film transfer coefficient in gold adsorption
- ψ shape factor of particles
- d' average particle diameter

CHAPTER 1

RESEARCH ORIENTATION

Summary

This chapter starts by giving a brief background to the history of activated carbon, a definition of activated carbon, as well as the main applications of activated carbon today. This is followed by a broad perspective of the different types of manufacturing of activated carbon.

1.1 History of Activated Carbon

Activated carbon in the form of carbonised wood can be traced back many centuries. Around 1500 BC the Egyptians used activated carbon as an adsorbent for medicinal purposes and also as a purifying agent. The ancient Hindus in India filtered their drinking water through charcoal.

It was only in the beginning of the twentieth century that the basis for industrial production of activated carbon was laid when it was used in 1900-1901 to replace bone char in the sugar refining process. This carbon was prepared by carbonising a mixture of materials of vegetable origin in the presence of metal chlorides or by the action of carbon dioxide or steam on charred materials.¹

1.2 Definition of Activated Carbon

The name activated carbon is given to carbonaceous materials with large adsorption capacity manufactured from a large number of materials.

The porous structure of an activated carbon is a function of the raw material used in its preparation, the activation method used and the extent of activation.

Activated carbons can be in either granular or powdered form. The granular active carbons are more abrasive resistant.

1.3 Main Applications of Activated Carbon

Due to the excellent adsorption properties activated carbon has found a variety of uses in almost every aspect of modern day society. Main applications of activated carbon are listed in Table 1.1.

<u>Application</u>	<u>Type of industry</u>	<u>Example of substances adsorbed</u>
Air purification	Rubber and paint	Waste gases
	Nuclear	Radio active vapours, iodine
	Chemical	Various hydrocarbons
Water purification	Municipal waterworks	Organic chemicals, toxic substances
Metal recovery	Mining	Gold, silver, copper
Decolourising	Food and beverage	Surface-active agents, phenol
Antidote, Activated carbon filters	Medicine	Bacterial toxins, nicotine
Gas masks	Defence	Toxic gases
Catalyst	Chemistry and engineering	Synthesis of various compounds

Table 1.1 Main applications of activated carbon

Of the above-mentioned industrial applications the mining sector and specific the gold mining industry is the largest user of activated carbon. In a market analysis done of the South African market the total average yearly estimated consumption was in the order of 4860 tons per annum. The most important characteristics of activated carbon used in gold recovery are size distribution and platelets contents. The specifications for the activated carbon are given in Table 1.2.²

Ash content (%)	I ₂ number (mg I ₂ per gram carbon)	Particle size distribution (mm)	Platelets (%)
2-4	1000 - 1200	1.18 - 2.8	> 5

Table 1.2 Specifications for activated carbon to be used in the gold recovery industry

1.4 Manufacture of Activated Carbon

Activated carbon can be manufactured from any carbonaceous raw material. Numerous patents have been granted for processes using such diverse starting materials as various ranks of coal (peat, lignite, bituminous coal and anthracite), coconut shells, peach and apricot stones, waste tires, wood, sawdust, petroleum heavy oil, cellulose, rice husks and many more.³⁻⁵ In practice five different types of carbonaceous materials are being used for industrial-scale production of activated carbons. These raw materials in the order of their importance and in terms of activated carbon production capacity are given in Table 1.3⁶.

Wood	130 000
Coal	100 000
Lignite	50 000
Coconut shell	35 000
Peat	35 000
Other	10 000

Table 1.3 Raw materials used for activated carbon in order of importance (tons / year)

The manufacture of activated carbon involves two main steps: the carbonisation of the carbonaceous materials followed by the activation of the carbonised product. The properties of the final product will differ depending on the nature of the raw material and the nature of the activating agent used as well as the conditions of the activation process.

1.4.1 Carbonisation

In the carbonisation step the starting material is heated in an inert atmosphere. Most of the volatile components are then driven off. The fixed carbon mass (known as a char) that is formed has a low surface area and a rudimentary pore structure.

1.4.2 Activation

The idea behind activation is not only to better the volume and to increase the diameters of the pores that were formed during the carbonisation process as described in 1.4.1, but also to create some new porosity.

The activation process can be divided into various phases. During the initial phase of activation the activation removes disorganised carbon and in doing so exposes the aromatic sheets to the action of activating agents that leads to the formation of a micro-porous structure. In the later phases of the activation process the existing pores are widened or large sized pores can even be formed when there is a complete burn out of the walls between adjacent pores.

There are mainly two methods of activation used in the production of activated carbon.

1.4.2.1 Chemical Activation

The chemical activation process combines the two steps of carbonisation and activation into one. This type of activation is usually carried out when the precursor is of a wood origin.

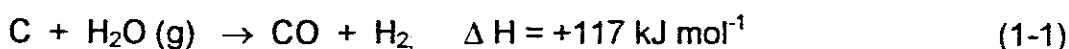
With chemical activation the precursor is impregnated with the activating agent in the form of a concentrated solution. The most widely used activating agents are phosphoric acid, zinc chloride and sulphuric acid, although potassium sulphide, potassium thiocyanate hydroxides and carbonates of alkali metals, chlorides of calcium, magnesium and ferric iron have also been suggested.⁷

1.4.2.2 Physical Activation

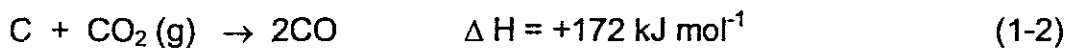
This type of activation is generally carried out at temperatures of between 1073 and 1373 K in the presence of various oxidizing gases like steam, carbon dioxide, air or any combination of these gases.

The type of gas employed for the gasification process has a significant impact on the eventual porosity development. This can be understood in terms of the following rationale:

The reaction of carbon with water vapour (gasification reaction) is endothermic



The same applies for the reaction of carbon with CO₂.



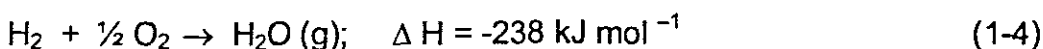
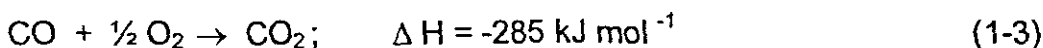
Both of the above reactions show strong product inhibition. The CO produced is chemically adsorbed onto part of the active sites and thereby inhibit product formation due to a decrease in the number of active points.

The CO₂ molecule has a larger dimension compared to that of H₂O. This results in the following:

- There is a slower diffusion into the porous system of the carbon.
- There is restricted accessibility towards the micropores.
- The rate of the gasification reaction is significantly lower.

For these reasons it is generally accepted that if CO₂ is employed as gasification reagent a better-developed mesoporous structure would result than if H₂O was to be utilised as gasification reagent.

Because reactions 1-1 and 1-2 are endothermic, heat can be supplied in order to maintain an isothermal situation. This is achieved by burning off the product gases via air in situ according to the following reactions:



These reactions facilitate the gasification reaction by increasing the effective partial pressure of the activation agent and by decreasing the partial pressure of the inhibiting product gases.

1.5 Contribution of this study

During previous research the activation of green medium temperature pitch (MTP) coke was investigated. After completing this research the conclusion was reached that this precursor would not give sufficient results in the gold market as well as the water purification market.

As an extension of the work on the green MTP coke it was decided to investigate the activation characteristics of different Sasol cokes in more detail. Of the total consumption of activated carbon in the South African market $\approx 70.4\%$ is used in the gold industry in their CIP process. The idea is to establish if activated carbon derived from "Smartie" coke as precursor would not only be suitable in the water purification market sectors, but also for use in the gold extraction process (CIP).

With the gold market in mind it was tried to activate calcined waxy oil coke with steam in both the fluidised bed and rotary kiln. It was not possible to produce activated carbon from this precursor. Consequently the activation of green "Smartie" coke (a mixture of MTP and waxy coke) is investigated.

This “new” precursor will be activated in both a fluidised bed reactor as well as a rotary kiln. This coke will combine the high reactivity (due to iron impurities) of the waxy oil and the high shock resistance of the green MTP coke.

The best results will then be tested for gold adsorption as well as water purification applications.

1.6 Objectives of the study

- Activate green Smartie coke in a rotary kiln
- Activate green Smartie coke in a fluidised bed reactor
- Characterise the prepared activated carbon
- Test the activated carbon for use in the gold as well as water purification industry

CHAPTER 2

THEORETICAL FOUNDATION FOR CHARACTERISATION TECHNIQUES

Summary

In this chapter the techniques used for characterisation of the activated carbon will be discussed. It will start off by giving a brief description of characterisation followed by an explanation of the adsorption processes. Lastly the various theories surrounding the characterisation and determination of the pore sizes will be discussed. As a large amount of topics are to be discussed in this chapter, it is presented as a broad survey that connects the background literature of the various components of the project.

2 Characterisation of activated carbon**2.1 Introduction**

When considering the characterisation of activated carbon there are two main properties that needs to be addressed: the available surface area of the solid onto which adsorption can take place and information on the pore structure of the solid.

2.2 Structure of activated carbon

X-ray analysis of activated carbons shows a structure which is much more disordered than that of graphite, having crystallites only a few layers in thickness and less than 10 nm in width⁷. The spaces between the crystallites of activated carbon constitute the micro porous structure with a large internal surface to which it owes its remarkable adsorption properties⁸.

2.3 N₂ adsorption isotherms

An adsorption isotherm is a measure of the molar quantity of gas n (or standard volume V_a) taken up, or released, at a constant temperature T by an initially clean solid surface as

a function of gas pressure P . This test is most often conducted at a cryogenic temperature, usually that of liquid nitrogen at its boiling point (77.35 K at one atmospheric pressure).

Although there are today six basic adsorption isotherms, it was Brunauer that first assigned type numbers to the first five isotherms⁹. The sixth isotherm is a very rare isotherm and is indicative of a nonporous solid with an almost completely uniform surface. The 6 types of isotherms found are shown in Figure 2.1

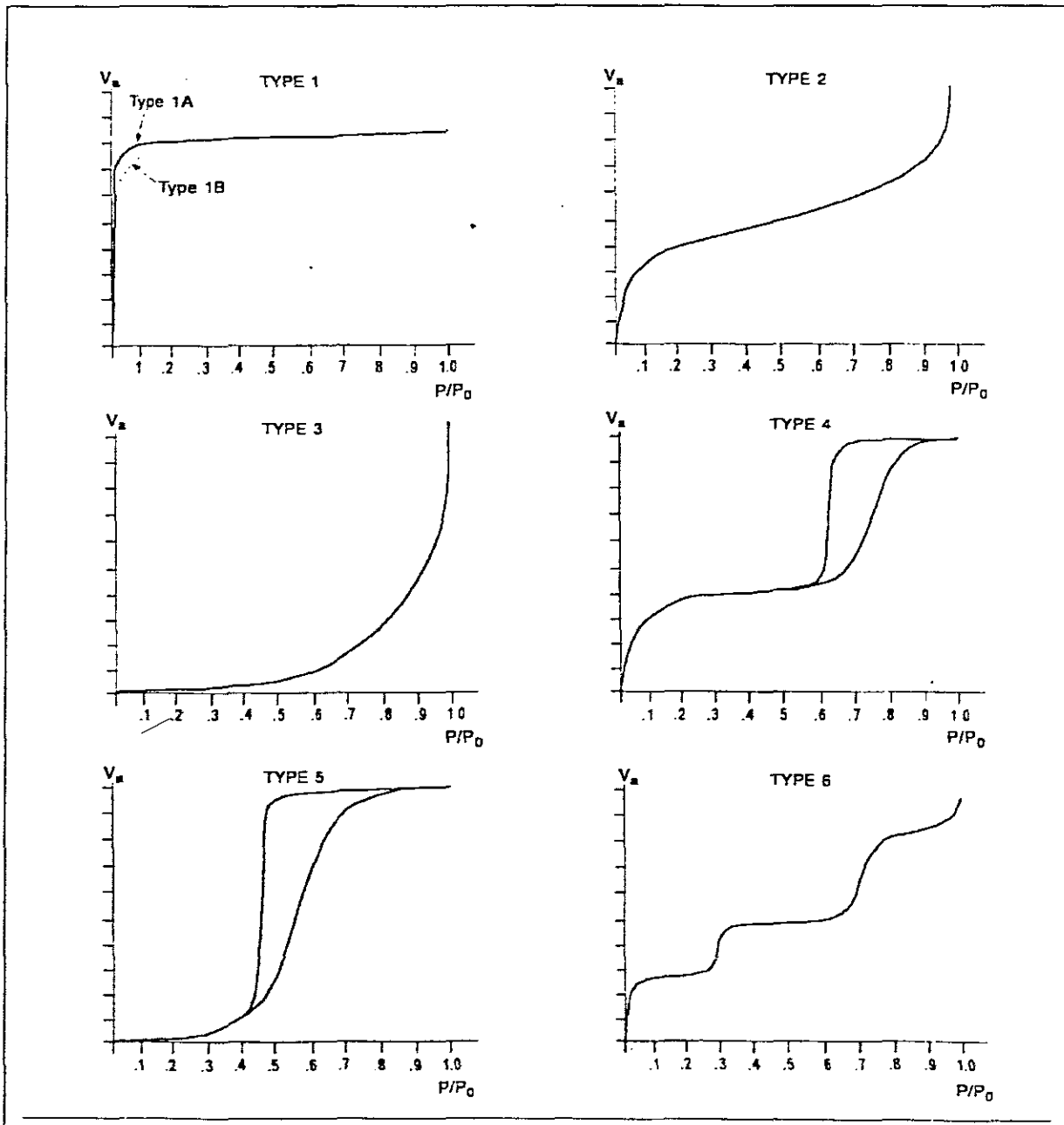


Figure 2.1 The six basic adsorption isotherm types

The shape of the adsorption isotherms can be explained as follows¹⁰. The initial rise in the curves are due to adsorbing of molecules interacting first with the most energetic regions

of the solid surface and then with less energetic regions. The isotherm with a more rounded knee (Type 1B) suggest that the activated carbon contain narrow micropores (steep initial branch) as well as wider micropores. The slope that can be observed at larger relative pressures (for example Types 2 and 4) is due to capillary condensation in the larger mesopores. Reversing the procedure by reducing the relative pressure leads to the formation of a wide hysteresis loop (Type 4). The occurrence of the hysteresis loop indicates that evaporation from a pore is a different process from condensation within it. Gas condensates build from the walls inward toward a central core of decreasing diameter. However, it evaporates from a liquid surface with a quite different curvature. This inhibits the evaporation and causes the decreasing portion of the loop to lag behind until all pores have been emptied. If no slope is observed (Type 1) the activated carbon has a predominant microporous structure.

2.4 Pore size distribution

A wide range of pore sizes forms the total porous structure of an activated carbon. For practical reasons the International Union of Pure and Applied Chemistry (IUPAC)¹¹ classify them into three ranges according to their width:

Micropores: less than 20 Ångstroms

Mesopores: between 20 and 500 Ångstroms

Macropores: more than 500 Ångstroms

The macropores of an activated carbon act as transport pores, enabling the molecules of the adsorptive to reach the smaller pores situated in the interior of the carbon particle. Thus, the macropores are not important from the point of view of the amount adsorbed in them, since their surface area is very low, but they affect the rate of diffusion into the meso- and micropores.

The mesopores that branch off from the macropores, serve as passages to the micropores for the adsorptive besides acting as pores where capillary condensation can take place. Normally the micropores constitute the largest part of the internal surface and, consequently, most of the adsorption takes place within them.

To achieve maximum effective use of activated carbon, various adsorption theories for activated carbon have been suggested.

2.4.1 The Langmuir Theory

In this theory it is assumed that gases form only a single molecular layer on a solid and that the collision of a gas molecule with a solid is inelastic. This causes the gas molecule to remain in contact with the solid for a time before returning back to the gas phase. This time delay is then taken as the reason for the occurrence of adsorption.

$$V_a = \frac{V_m b P}{1 + b P} \quad (2-1)$$

where V_a = quantity of gas adsorbed at pressure P

V_m = quantity of gas adsorbed when entire surface is covered with a monomolecular layer

b = empirical constant

Equation 2-1 was obtained by relating the rate at which molecules strike a surface to the rate at which they leave the surface.

When the values of $1/V_a$ are plotted against $1/P$, a straight line should result. The value of V_m can be obtained from the intercept and b from the slope of the line.

2.4.2 The BET Theory

Brunauer, Emmet and Teller generalized Langmuir's theory and incorporated the concept of multi-molecular layer adsorption. The basic assumption made was that forces that are active in the condensation of gas molecules are also responsible for the binding energy in multi-molecular adsorption. The BET equation (named after the surnames of its originators)¹² is:

$$SA = \frac{V_M}{22414} N_a * \alpha \quad (2-2)$$

where N_a is Avogadro's number

V_M is the monolayer coverage

α is the area covered by one molecule of N_2

α can be determined by Equation 2-3. In Equation 2-3 ρ is the density of the adsorbed phase, which is almost equal to the liquid density ($\rho_{N_2, -195.8^\circ C} = 0.808 \text{ g cm}^{-3}$) and M is the molecular mass of the adsorbent.

$$\alpha = 1.09 \left(\frac{M}{Na \cdot \rho} \right)^{2/3} \quad (2-3)$$

The major criticism against the use of the BET equation is that it treats all adsorption sites as identically energetic. It therefore neglects the interactions between adjacent adsorbate molecules in the same layer. It also does not take into account the diminution of the adsorption forces as the outer layers build up and the distance from the surface therefore increases.

Despite these criticisms it is still a widely used theory for the evaluation of surface areas.

2.5 Estimation of the micropore volume

2.5.1 The Dubinin-Radushkevich (DR) equation

Dubinin and Radushkevich put forward an equation to estimate the micropore volume from the low and medium-pressure parts of the adsorption isotherm.¹³ The equation is based on the Polanyi theory of adsorption potentials, and assumes that the degree of the filling of the micropores is a function of the adsorption potential. The mathematical form of the DR - equation is:

$$V = V_0 e^{-(A/E)^2} \quad (2-4)$$

where	V	=	amount adsorbed (ml / g)
	V_0	=	liquid micropore volume (ml / g)
	A	=	adsorption potential
		=	$RT \ln(p_0 / p)$
	E	=	energy parameter

Substituting the adsorption potential $RT \ln(p_0 / p)$ for A in Equation 2-4, the DR-equation can be rewritten as

$$\ln V = \ln V_0 - \xi \ln^2 (p_0 / p) \quad (2-5)$$

with ξ a constant. A plot of $\ln V$ against $\ln^2 (p_0 / p)$ should yield a straight line with an intercept equal to the logarithmic value of the micropore volume.

There are however a few uncertainties regarding the extrapolation of the DR plots to $\ln^2 (p_0 / p) = 0$. Certain deviations tend to take place under the following conditions and in some cases to such an extent that the experimental data do not at all fit the DR-equation:

- ◆ When the activation is very high and micropore size distribution is very wide and
- ◆ when the data obtained goes above relative pressures of 0.1 - 0.2

2.5.2 Dubinin-Astakhov (DA) Equation

Because there are uncertainties in the extrapolation of the DR equation plots Dubinin and co-workers have attempted to extend the scope of the DR equation developing more general equations.¹⁴⁻¹⁶ While Dubinin-Radushkevich based their equation on a gaussian distribution of pore sizes, Dubinin and Astakhof based their work on a Weibull distribution.

They therefore obtained the following equation:

$$V = V_0 e^{-(A/E)^n} \quad (2-6)$$

Here n is selected to give the best linear regression fit with its value usually between 1 and 3. Very often it is near to 2. It can then be said that the DR equation is a special case of the Dubinin-Astakhof equation, with $n = 2$.

The surface characteristic energy E_0 , and the structural heterogeneity parameter, n , can be calculated by a non-linear least square fit of the experimental data into the DA equation, and using 0.34 as the β factor.

$$\ln\left(\frac{V_{ads}}{V_M}\right) = -\exp\left(\frac{A}{\beta E_0}\right)^n \quad (2-7)$$

where

$$A = RT \ln\left(\frac{p_0}{p}\right) = -\Delta G \quad (2-8)$$

V_M is the monolayer capacity and V_{ads} is the quantity adsorbed at relative pressure p/p_0 . The limiting micropore volume, V_0 , is calculated from Equation 2-9.

$$V_0 = V_M \times D; \text{ where } D = \text{density conversion factor (cm}^3 \text{ liquid/cm}^3 \text{ STP)} \quad (2-9)$$

2.5.3 Density functional theory (DFT)

In this study the DFT based software was used to automatically determine the pore size distribution. In the DFT calculations it is assumed that the pores are slit shaped. The idealized physical model conventionally accepted for micropores in carbons is that of the slit. This is based on the presence of graphitic-like layer planes as the upper and lower bounds of the slit.

In terms of geometry the simplest system to model is that of a single pore represented by two parallel walls separated by a distance H . The pore is open and immersed in a single component fluid (adsorptive) at a fixed temperature and pressure. Under such conditions, the fluid responds to the walls and reaches equilibrium. In this condition (by definition of equilibrium), the chemical potential at every point in the fluid equals the chemical potential of the bulk fluid. As the bulk fluid is a homogeneous system of constant density its chemical potential can be determined by the pressure of the system.

The fluid near the walls is not of constant density. Its chemical potential is made up from several density-dependent contributions. At equilibrium these contributions must total at every point to the same value as the chemical potential of the bulk fluid.

At equilibrium the system has a minimum free energy. This is thermodynamically known as the grand potential energy and is expressed as:

$$W[\rho(r)] = F[\rho(r)] + \int dr \rho(r) (V(r) - \mu) \quad (2-10)$$

where

$\rho(r)$ = equilibrium density at a general 3-space co-ordinate r

$V(r)$ = potential acting on a molecule at r

μ = chemical potential

F = free energy expressed as a function $F[\rho(r)]$ of the molecular density distribution at equilibrium

Equation 2-10 describes (in terms of energy and molecular population density) a system of atoms and molecules at a specific temperature and pressure and associated with a specific pore size¹⁷.

2.5.4 T-Plot

A variety of materials of different total surface areas have similar isotherm curves when analysed with the same adsorptive at the same temperature. This idea has led to the concept of a standard isotherm applicable to a specific group of materials in such categories as metal oxides, metals, graphite, metal halides and silicas¹⁸. This in return led to a way of determining the volume of micropores and detecting the presence of mesopores.

2.6 GOLD ADSORPTION

2.6.1 Introduction

Already in 1880 in Australia Davis patented a process for the recovery of gold by adsorption on a wood charcoal from chlorination leach solutions.¹⁹ Not long after that Johnson suggested that wood charcoal could be used for the adsorption of gold from cyanide leach liquors.²⁰ He made this suggestion after it was recognised that cyanide was a better solvent for gold.

Even though these workers continued their work on the subject the process was not economically viable. The charcoals that they used for their investigations did not have the pore structures of the carbons of today. Another reason for their limited success was that the only method known to them to elute the gold from the carbon was to burn the charcoal to ash. Due to the fact that the ash was in most cases much more than the gold it made the recovery process very difficult.

It was not until the early 1950's that carbon was used to recover gold. During these years Zadra et al of the U. S. Bureau of mines developed the direct carbon- in - pulp (CIP) process. In this process the carbon granules are directly added to the cyanide pulp and moved countercurrent to it.^{21, 22} The gold loaded carbon was then recovered by screening.

CIP technology was employed when the Homestakes Mining Company built the first commercial plant for large-scale recovery of gold in the United States.²³ Most of the larger mines use CIP plants for the recovery of gold.

2.6.2 Mechanism of gold adsorption

Since 1913 the mechanism by which activated carbon extracts $AC(CN)_2^-$ from aqueous solutions has interested and puzzled researchers. Even though this has a great influence on the commercial success of the CIP process no consensus has as yet been reached and continues to be a great topic for debate.²⁴

These differences can be greatly described to the fact that activated carbon cannot be directly investigated by techniques such as infrared and ultraviolet-visible spectroscopy. Together with this is the fact that the recorded investigations were not done on the same activated carbons that were activated under the same conditions. In addition the activated carbons were also loaded with $\text{Au}(\text{CN})_2^-$ under different experimental conditions.

The various mechanisms of gold adsorption from cyanide solution proposed in the literature generally fall into one of the following six categories:²⁵⁻²⁷

- the reduction of $\text{Au}(\text{CN})_2^-$ to metallic gold,
- the adsorption of $[\text{M}^{n+}][\text{Au}(\text{CN})_2]_n$ ion pairs,
- the electrical double-layer adsorption of $\text{Au}(\text{CN})_2^-$ anions and cations onto a charged surface,
- the ion exchange extraction of $\text{Au}(\text{CN})_2^-$ anions by positively charged carbonium-ion sites which were postulated to exist on the surface of the carbon,
- the adsorption of $\text{Au}(\text{CN})_2^-$ species with subsequent degradation to the AuCN polymeric species, and
- the adsorption of ion pairs followed by partial reduction of the $\text{Au}(\text{CN})_2^-$ complex to a cluster-type species.

The total amount of evidence that has been compiled from all the experiments conducted favours a mechanism in which the $\text{Au}(\text{CN})_2^-$ anion is adsorbed without chemical change. The 'ion-pair' adsorption reaction mechanism has been vigorously advocated by various researchers²⁸⁻³⁴.

The above researchers gathered together a lot of evidence to support this mechanism as the main one responsible for the adsorption of gold di-cyanide onto activated carbon. They maintain that gold is adsorbed onto the carbon surface as the neutral 'ion-pair' $[\text{M}^{n+}][\text{Au}(\text{CN})_2]$

2.6.3 Factors influencing gold adsorption on activated carbon

There are quite a few factors that have to be taken into consideration when determining the capacity for gold adsorption of a specific activated carbon. These factors all have an influence on the mechanism and kinetics of the gold adsorption onto the activated carbon. Various researchers³⁵⁻³⁷ did experimental work based on the above statement and their conclusions are summarized in the following sections.

2.6.3.1 Effect of pore size distribution on gold adsorption

In her studies Voges showed that a difference in the pore structure of an activated carbon has a profound influence on the adsorption capabilities of the specific activated carbon³⁸. This was especially evident when experiments were conducted under different pH conditions.

Voges found that a higher micropore area produced a higher equilibrium loading during equilibrium tests. Although most carbons will adsorb gold, the carbon therefore preferred for gold adsorption is one with a high BET surface area and a high micropore volume.

2.6.3.2 Effect of oxygen and surface oxygen functional groups

Substituent groups or impurities on a carbon surface could cause less adsorption if these groups should repel or fail to attract the molecules of the adsorbate. An important class of substituents on porous activated carbon is the surface oxides that is produced by the chemisorption of oxygen.

Oxygen has a very important role to play in the adsorption process and this has been shown by various researchers.^{35, 36,39} Dixon et al found that there was a decrease in the amount of gold loaded onto the carbon when a nitrogen environment was maintained during the adsorption process. Van der Merwe and Van Deventer found that the amount of gold loaded decreased when the oxygen in the solution fell below 8 mg/l.

As early as 1863 Smith suggested that when oxygen is adsorbed on a carbon surface it undergoes a chemical change⁴⁰. Rhead and Wheeler pointed out that oxygen combines with the carbon to form a physico-chemical complex, C_xO_y of variable composition^{41,42}. This complex decomposes upon heating giving a carbon monoxide and carbon dioxide mixture.

Despite a large amount of information that have been gathered by either direct or indirect methods,^{43 - 45} the structure of the surface oxides has not yet been completely clarified. In their research of both direct and indirect methods Ishizaki and Marti reached a conclusion that a mixture of oxide structures exist in activated carbons with the main surface oxides being lactones, quinones, phenols and carboxylates⁴⁶

2.6.3.3 Effect of other anions and cations in solution

During the adsorption process complex cyanides are also adsorbed onto the carbon. This lowers the gold loading onto the carbon.

The effect of these anions is in the following order:



In opposition to the anions present the adsorption of gold is enhanced by the presence of cations in the solution, especially CaCl_2 . The effect of these cations is in the following order:



2.6.3.4 Effect of pH

There is a strong increase of adsorption in a pH range of 5 and less. In this acid medium it has however been found that toxic HCN gas may be liberated and it is for this reason then that CIP plants prefer to operate at pH levels of above 9. It has also been found that adsorption is also almost completely independent of pH levels of between 6 and 12.

2.6.4 Kinetics of gold cyanide adsorption

Various researchers have proposed a first order equation for modeling the adsorption of gold cyanide onto activated carbon^{47 - 49}. The rate of adsorption can be written from the liquid phase material balance as :

$$-\frac{d[\text{Au}]}{dt} = k \{ [\text{Au}] - [\text{Au}]_c \} \quad (2-11)$$

[s1] where $[\text{Au}]$ = gold concentration in the bulk solution, (mg / dm³)

$[\text{Au}]_c$ = gold concentration on the carbon surface (mg / dm³)

k = observed rate constant

For a reaction controlled by film diffusion $[\text{Au}]_c$ is negligible, so that integration of Equation 2-11 yields:

$$\ln[\text{Au}] = \ln[\text{Au}]_o - kt \quad (2-12)$$

where $[\text{Au}]$ = gold concentration in the bulk solution at time t , (mg / dm³)

$[\text{Au}]_o$ = initial concentration of gold in the solution, (mg / dm³)

t = duration of adsorption, (min)

Equation 2-12 is the rate expression used commonly in batch reactor kinetic studies.

The observed rate constant k is related to the film transfer coefficient k_f by the equation:⁴³

$$k = \frac{6M\psi k_f}{d'\rho V'} \quad (2-13)$$

- where k_f = film transfer coefficient
- M = mass of activated carbon
- ψ = shape factor of particles, spherical = 1
- d' = average particle diameter
- ρ = density of carbon particles
- V' = volume of solution

2.7 Summary of characterisation methods used in this study

Table 2.1 is a summary of all the characterisation methods used in this study.

Method used	Calculated Parameters	Information gained
Gas adsorption (N ₂ at 77K)		Pore size distribution
BET equation (2-2)	SA	Total surface area
DA equation (2-6)	E_0, V_0, n	Characteristic energy, liquid micropore volume, structural heterogeneity parameter
Gold adsorption	k_f	Rate of adsorption

Table 2.1 Summary of characterisation methods used

CHAPTER 3**EXPERIMENTAL****Summary**

In this chapter the experimental procedures will be described in detail. This will be followed by a description of how the experimental data for the characterization of the activated carbon was obtained. Finally the gold adsorption tests and water purification experiments will be discussed.

3.1 Reagents

Reagent grade chemicals were used in all cases.

3.2 Physical activation

“Smartie” coke was obtained from the Carbo Tar division of Sasol (Pty) Ltd. The samples were ground and the 1 - 2.36 mm size fraction was sieved out.

A schematic drawing of the experimental rig for activation in the rotary kiln is given in Figure 3.1. A photo of the rig is given in Figure 3.2.

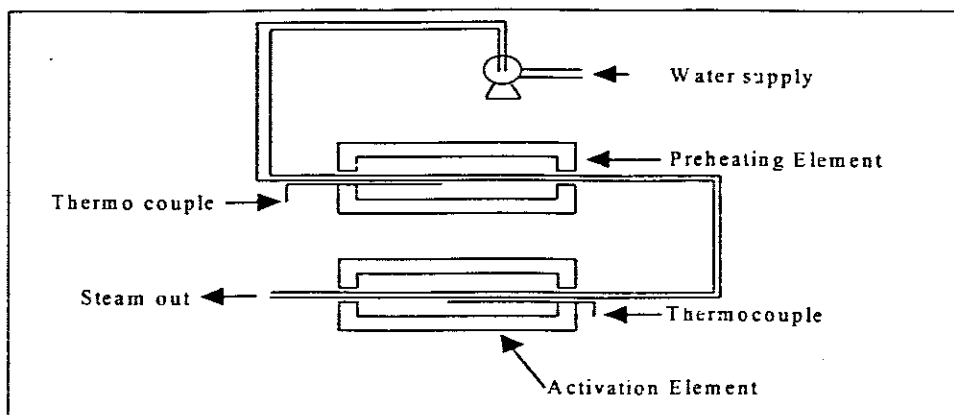


Figure 3.1 Schematic drawing of rig for activation in laboratory rotary kiln.

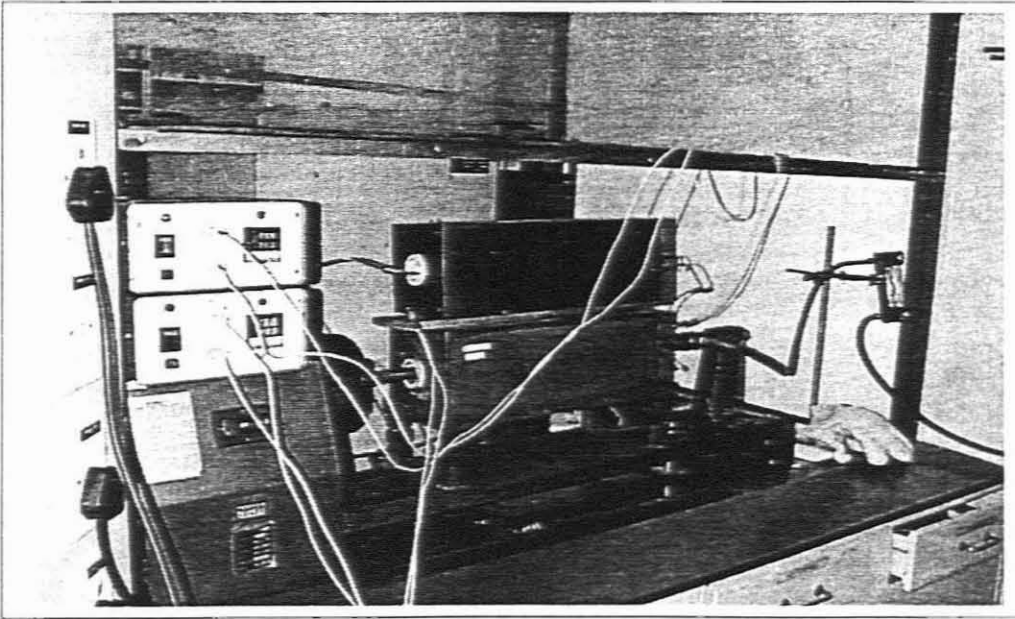


Figure 3.2 Experimental rig for activation in a rotary kiln

Rotary kilns are widely employed for activation but they are energy intensive and they lack good gas-solid contact. Their main advantage is the regulation of the temperature at different temperature zones; and in this respect they can be more suitable for activation processes. Rotary kilns also are easy to construct and to operate.

Activation in the laboratory scale kiln was performed as follows:

A 15 g sample of coke was loaded into a stainless steel cylinder and inserted into an external electric heater. The cylinder was heated and concurrently a constant flow of nitrogen was passed through it until the desired temperature was reached. Once at the predetermined temperature the nitrogen was replaced by superheated steam to commence the activation. The steam flow was kept constant for the desired period of activation. Once the desired activation time was reached, the steam was replaced with nitrogen, the elements were switched off and the sample was allowed to cool down. The sample was removed from the cylinder and weighed. The carbon conversion was determined from Equation 3-1.

$$X = \left(\frac{W_0 - W_t}{W_0 - W_{ash}} \right) \times 100 \quad (3-1)$$

where W_0 = mass before activation, W_t = mass after activation, W_{ash} = mass at 100 % carbon conversion.

The gasification rate was calculated from the experimental data (mass loss as function of burn-off) from the following equation:

$$r = \frac{dX}{1-X} dt \quad (3-2)$$

where t = time.

It is possible to perform a kinetic analysis of the carbon gasification rate by fitting the experimental carbon conversions to different models⁵⁰⁻⁵⁴. Reaction rate expressions and a short description of two theories that were applied in this investigation are given in Table 3.1.

Model	Description of model	Reaction rate expression
Shrinking core	Reacting char particles are considered as spherical grains whose radius decreases as the gasification reaction advances.	$X = 1 - (1-tk)^3$ (1)
Random pore	Random overlapping of pores' surfaces, which reduce the area available for reaction.	$X = 1 - \exp[-2\pi(A_0t + 2A_1)]$ (2)

Table 3.1 Kinetic models for char gasification reaction

A schematic drawing of the experimental rig for activation in the fluidised bed (FB) is given in Figure 3.3. A photo of the rig is given in Figure 3.4.

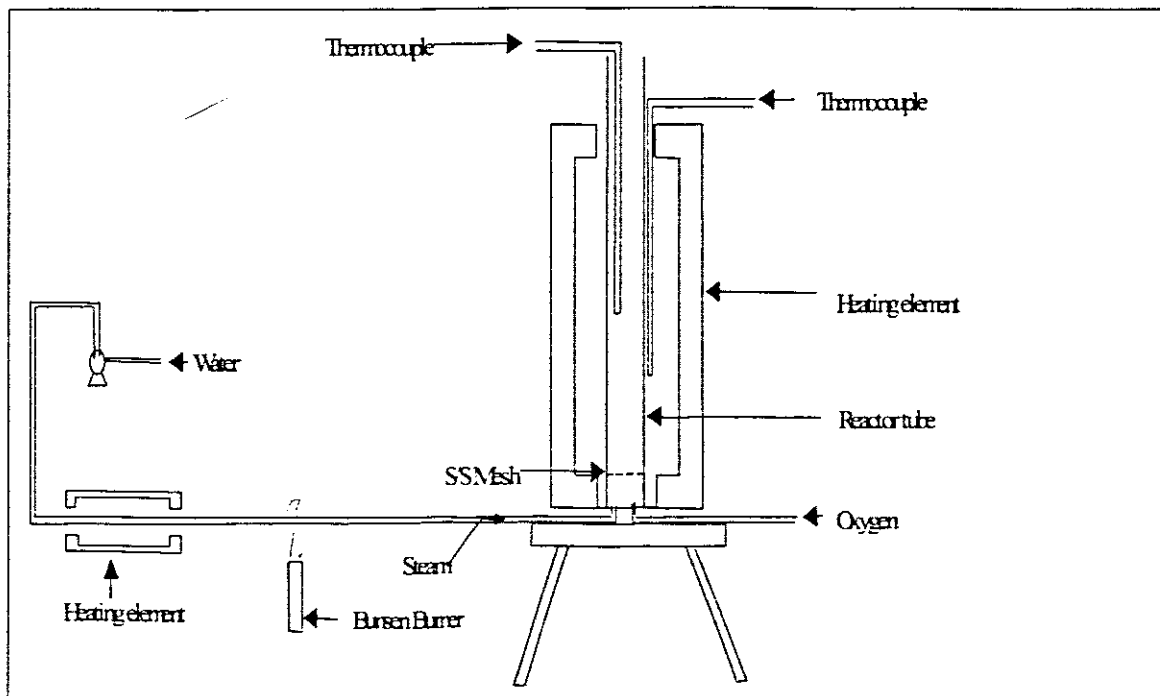


Figure 3.3 Schematic drawing of rig for activation in FB

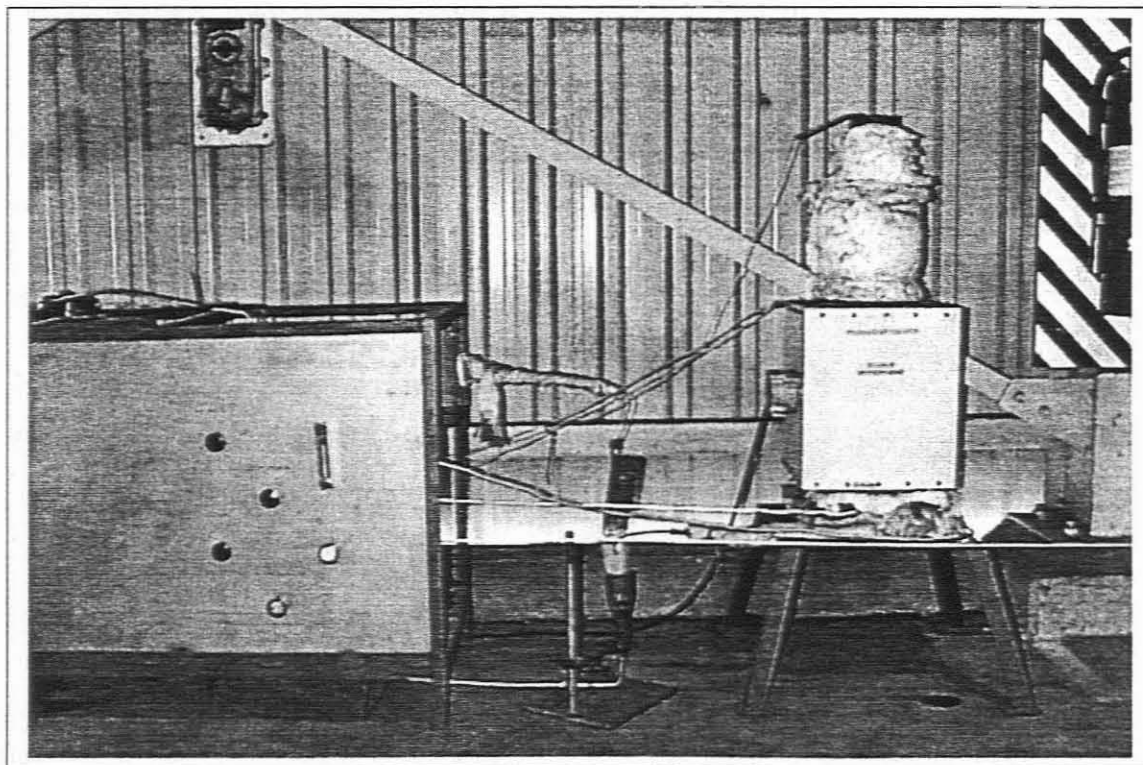


Figure 3.4 Experimental rig for activation in a fluidised bed reactor

The production of activated carbon involves a gas-solid reaction, and a reactor with better contacting of the phases and good transport processes is essential. Fluidised beds are well-known for their excellent gas-solid contact and high heat and mass transfer rates. The vigorous gas-solid contact in a fluidised bed aids the reaction and also removes the waste gaseous products from the vicinity of the solids during reaction, thus exposing the solid reactant to the fresh incoming gaseous reactants. Unfortunately, fluidised beds do not readily lend themselves as single units to staged processing at different temperatures; as is required for drying, devolatilisation, charring and the steam-carbon reaction. Fluidised beds are also known to cause more attrition of the feed than rotary kilns and multiple hearth furnaces. Moreover, they are not feasible for the activation of coarse particles. Despite these disadvantages, activation in fluidised beds remains attractive because products having large surface areas can be obtained from them.

Activation in the FB was performed as follows:

The FB was preheated under a flowing stream of nitrogen to the desired activation temperature employing an external electric heater. Once the temperature was reached the FB was charged with 200 g of "Smartie" coke, while the nitrogen was still allowed to flow in order to facilitate the pyrolysis of the "Smartie" coke. When the pyrolysis was complete and the temperature has stabilised (during pyrolysis there was a slight drop in

temperature) superheated steam was added to fluidise the coke. Samples were taken at one hour intervals and stored in sample containers for further analysis.

The activation was performed under the following conditions : 0.5 hour < heat treatment time (HTt) < 7 hours and 700°C < temperature < 900°C.

3.3 Characterisation

The determination of the metal content of the "Smartie" coke was performed on a Vista AZ CCD simultaneous ICP-AES instrument. Prior to the ICP measurements the coke sample was placed in a silica crucible and ashed at 873 K until all the carbon was burned away. To ~0.4 g of cooled down ash was added 4 cm³ of concentrated sulphuric and 15 cm³ hydrofluoric acid. This mixture was placed on a hot plate and it was evaporated to ~1 cm³. After the mixture was cooled down it was transferred to a large beaker and 10 cm³ HCl was added. The mixture was again evaporated to ~10 cm³ to facilitate complete solution of the metals. It was then diluted to 250 cm³ and the undissolved residues were filtered out. Consequently 10 cm³ of this filtrate was diluted to 100 cm³ and the metal content was determined on the ICP instrument.

Proximate analysis was conducted on a Perkin Elmer TGA. 10 – 20 mg sample was placed in a platinum crucible. The sample was heated at 50°C min⁻¹ up to 873 K under a constant flow of nitrogen (flow rate = 183 cm³ min⁻¹ STP). At this stage the nitrogen was replaced with oxygen and heated further at the same heating rate up to 1273 K.

The activated carbon products were characterised mainly by determining their iodine numbers. The latter is an indication of the surface area contributed by the pores larger than 10 Ångstroms.

A representative sample of the activated carbon was ground until 95% or more passed through a 45µm screen. The sieved sample was dried in a vacuum oven for three hours and then it was allowed to cool to room temperature in a dessicator. Approximately one gram of the sample was weighed off and 10 cm³ of a five percent HCl solution was added to it. The wetted mixture was brought to boiling point and left there for thirty seconds in order to remove sulphides, which might interfere with the subsequent determinations.

Once the mixture has cooled down to room temperature 100 cm³ of a 0.1 N iodine solution was added, shaken vigorously for 30 seconds and filtered by gravity. The first 20 - 30 cm³ was discarded and the remainder was collected in a beaker. 50 cm³ of the filtrate was

titrated against a standardised 0.1N sodium thiosulfate solution until the solution was a very pale yellow. Starch indicator was added and the titration was continued until one drop produced a colourless solution. The volume of $\text{Na}_2\text{S}_2\text{O}_3$ was recorded and the iodine number was calculated as follows:

$$\frac{X}{M} = \frac{A - 2.2 \times B \times C}{g} \quad (3-3)$$

X/M = milligram of iodine adsorbed per gram of carbon.

A = $N_1 \times 12693$; N_1 = normality of iodine solution

B = $N_2 \times 126.93$ and N_2 = normality of $\text{Na}_2\text{S}_2\text{O}_3$ solution

C = cm^3 of $\text{Na}_2\text{S}_2\text{O}_3$ used

g = mass of sample used in grams

3.4 BET and pore size distribution measurement

Nitrogen adsorption measurements were performed at 77 K using a static volumetric apparatus (Micromeritics ASAP 2010 adsorption analyser). The samples were degassed at 473 K for 24 hours and 0.133 Pascal before analysis. The BET surface area was calculated according to the procedure described in Section 2.4.2.

The pore size distribution was calculated from the nitrogen adsorption data at 77 K with the density functional theory (DFT) and utilizing the DFT software (Micromeritics) for slit-like micropores. The calculations of these were discussed in Section 2.5.3.

3.5 Gold adsorption tests

Potassium aurocyanide was used as an adsorbate. The "smartie" coke activated carbon was tested against an experimental coconut shell activated carbon (ANK).

Adsorption tests were performed in a perspex batch stirred tank. It had an internal diameter of 11 cm, a height of 15 cm and was fitted with three evenly spaced baffles of width 1 cm. Agitation was done by means of a magnetic stirrer. Equilibrium experiments were done in stirred vessels of 1 L each containing 10, 20, and 40 ppm of $\text{Au}(\text{CN})_2^-$ and 0.2g of carbon. Samples were taken at predetermined intervals and then analysed for

gold, so as to monitor the approach to the equilibrium. The pH was varied between 8 and 12 to monitor the effect of the varied pH on the adsorption curves.

A Varian Techtron AA-1275 atomic absorption spectrophotometer was used for the analysis of the metal cyanides.

A schematic drawing of the rig for the gold adsorption tests is given in Figure 3.5

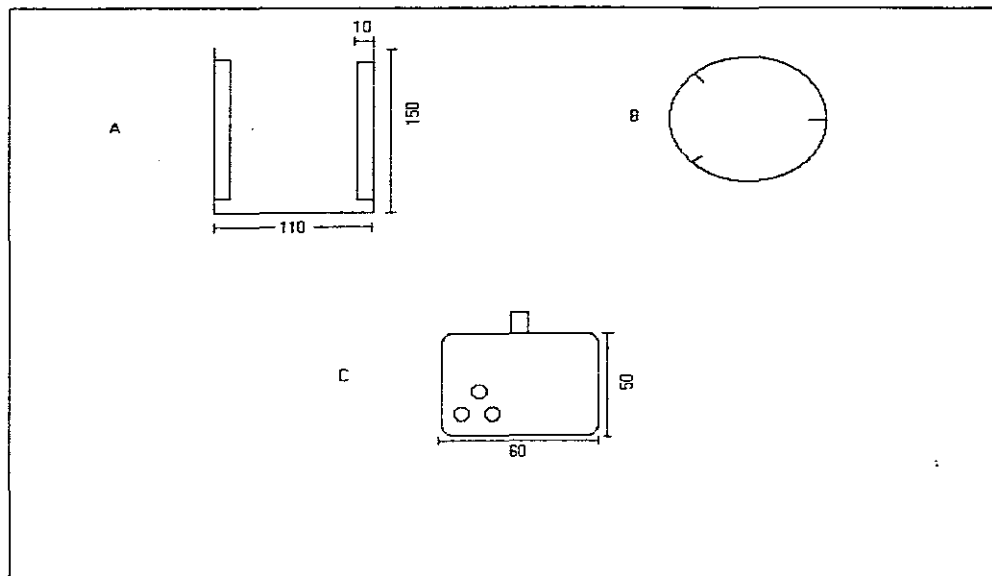


Figure 3.5 Schematic drawing of gold adsorption tests. A. Perspex reactor (side view), B top view, C flat blade impeller

3.6 Water purification tests

A water sample from a waste effluent stream from one of the industries in the Western Cape area was used for the purification tests.

3g activated carbon was put into 500 ml of the effluent water. This was then stirred continuously for 24 hours and samples were taken at intervals of 2, 6 and 24 hours. The samples were filtered before they were analysed. A dissolved organic content (DOC) test was performed on each of these samples.

The carbon samples that were used for the tests were the "smartie" coke activated carbon, ANK, and a wood based steam activated carbon D2-4.

CHAPTER 4

OPTIMISATION OF PROCESS PARAMETERS

4.1 Proximate and ICP analysis

Results of the proximate and ICP analysis on the “Smartie” coke are given in Table 4.1.

Ash (%)	Volatiles (%)	Moisture (%)	Fixed carbon (%)	Fe (%)
0.7	11.3	1	87	0.7

Table 4.1 Characteristics of the “Smartie” coke.

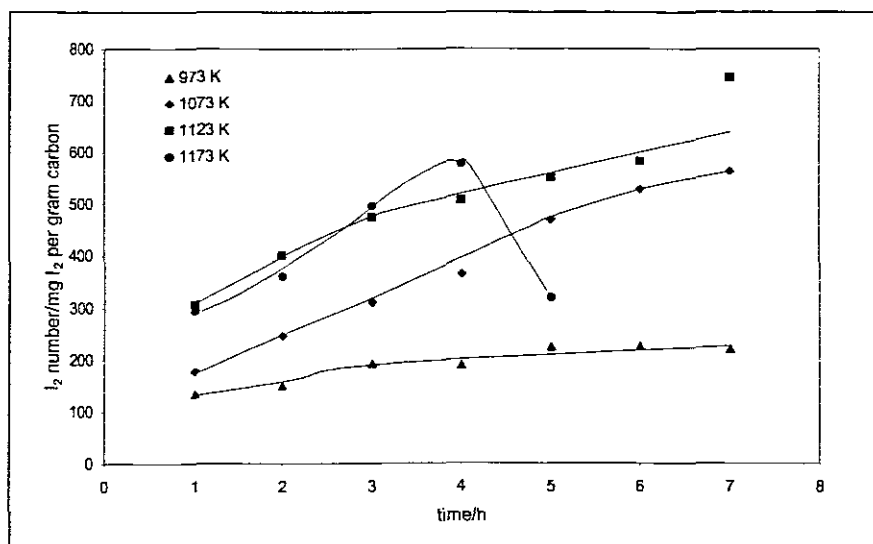
The results in Table 4.1 show that the ash content of the “Smartie” coke precursor is very low. This implies that the ash content of the activated carbons resulting from this precursor would also be low and consequently it would be possible to prepare an activated product from this precursor which has an application in “niche” markets such as food and beverage manufacturing. Due to the low ash content of the “Smartie” coke Sasol will have a competitive advantage if they could sell a coke derived activated carbon in South Africa. As was already stated, “Smartie” coke is a mixture of waxy oil and MTP coke (the MTP coke/waxy oil coke ratio is unknown). The characteristics of the waxy oil and MTP coke are combined in this precursor. The green MTP coke has a high shock resistance and consequently the activated carbon produced from the “Smartie” coke will be more abrasive resistant than activated carbon produced from waxy oil coke or petroleum pitch cokes. The iron content in the “Smartie” coke sample is due to the presence of waxy oil coke. It is expected that the iron would catalyse the steam gasification reaction and consequently the “Smartie” coke will be more reactive than the green MTP coke⁵⁵.

4.2 Iodine numbers and carbon conversion

As stated already, both fluidised bed and kiln technologies were utilised to activate the “Smartie” coke. In order to evaluate what activation conditions gave the best surface

areas the iodine numbers for each batch was measured. The best results were then taken and a BET analysis was done on these samples. Iodine numbers and BET total surface areas of the activated carbons produced in the kiln and fluidised bed reactors are given in Table 4.2 and iodine number versus time plots are given in Figure 4.1. By way of comparison, requirements of commercial activated carbons used in the industry are given in Table 4.3.

a.



b.

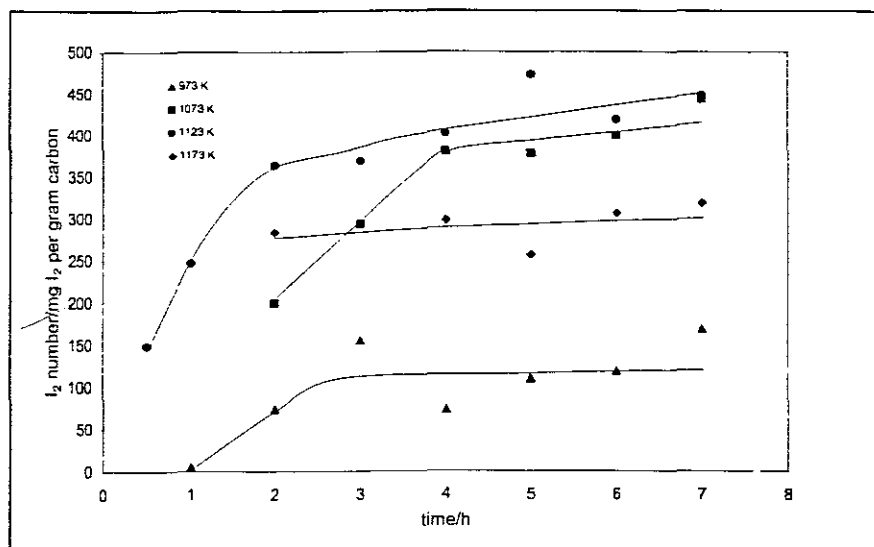


Figure 4.1 Iodine number versus heat treatment time.

Table4.2 Characteristics of Sasol activated carbons.

Reactor	T (K)	HTt (h ⁻¹)	LHSV (cm ³ g h ⁻¹)	I ₂ number (mg I ₂ per gram carbon)	BET (m ² g ⁻¹)	V ₀ (t-Plot) (cm ³ g ⁻¹)	V ₀ (H-K) (cm ³ g ⁻¹)	V ₀ (DA) (cm ³ g ⁻¹)	Meso= pore volume (BJH) (cm ³ g ⁻¹)	E ₀ (kJ mol ⁻¹)	n
FB	973	1	61.7	134.8							
		2		150.8							
		3		192.9	18.93	0.0072	0.0061	0.0233	0.0116	6.0275	1
		4		189.7	29.28	0.0138	0.0114	0.0255	0.0021	9.9269	1
		5		225.2							1
		6		227.4	49.37	0.0227	0.0201	0.0292	0.0034	21.1833	1
		7		221.1	68.13	0.0309	0.0267	0.0395	0.0051	21.299	1

Table 4.2 (Continued)

Reactor	T (K)	HTt (h ⁻¹)	LHSV (cm ³ g h ⁻¹)	I ₂ number (mg I ₂ per gram carbon)	BET (m ² g ⁻¹)	V ₀ (t-Plot) (cm ³ g ⁻¹)	V ₀ (H-K) (cm ³ g ⁻¹)	V ₀ (DA) (cm ³ g ⁻¹)	Meso= pore volume (BJH) (cm ³ g ⁻¹)	E ₀ (kJ mol ⁻¹)	n
FB	1073	1	68.0	178.3							
		2		246.8							
		3		310.7							
		4		364.1							
		5		469.1							
		6		528.3							
		7		563.5	404.44	0.1609	0.1459	0.1654	0.0816	22.624	2.1
FB	1123	1	71.0	306.1	120.6	0.0539	0.0459	0.0564	0.0123	24.293	1.6

Table 4.2 (Continued)

Reactor	T (K)	HTt (h ⁻¹)	LHSV (cm ³ g h ⁻¹)	I ₂ number (mg I ₂ per gram carbon)	BET (m ² g ⁻¹)	V ₀ (t-Plot) (cm ³ g ⁻¹)	V ₀ (H-K) (cm ³ g ⁻¹)	V ₀ (DA) (cm ³ g ⁻¹)	Meso= pore volume (BJH) (cm ³ g ⁻¹)	E ₀ (kJ mol ⁻¹)	n
FB	1123	2	71.0	399.8							
		3		474.0	329.34	0.1158	0.1116	0.1289	0.1021	21.552	2.1
		4		506.7	402.78	0.1268	0.1307	0.1505	0.1639	20.893	2.2
		5		550.1	473.24	0.1319	0.1493	0.1707	0.2417	20.426	2.4
		6		582.1	524.39	0.1336	0.1633	0.1862	0.3072	20.056	2.4
		7		745.2	445.76	0.0765	0.1201	0.1334	0.3740	19.684	2.8
FB	1173	1	74.3	294.2							
		2		360.2							

Table 4.2 (Continued)

Reactor	T (K)	HTt (h ⁻¹)	LHSV (cm ³ g h ⁻¹)	I ₂ number (mg I ₂ per gram carbon)	BET (m ² g ⁻¹)	V ₀ (t-Plot) (cm ³ g ⁻¹)	V ₀ (H-K) (cm ³ g ⁻¹)	V ₀ (DA) (cm ³ g ⁻¹)	Meso= pore volume (BJH) (cm ³ g ⁻¹)	E ₀ (kJ mol ⁻¹)	n
FB	1173	3	74.3	496.0							
		4		576.3	445.52	0.0699	0.1345	0.1499	0.4600	18.852	2.8
		5		319.9							
Kiln	973	2	5.68	74.2							
		3		155.4							
		4		73.0							
		5		109.7							

Table 4.2 (Continued)

Reactor	T (K)	HTt (h ⁻¹)	LHSV (cm ³ g h ⁻¹)	I ₂ number (mg I ₂ per gram carbon)	BET (m ² g ⁻¹)	V ₀ (t-Plot) (cm ³ g ⁻¹)	V ₀ (H-K) (cm ³ g ⁻¹)	V ₀ (DA) (cm ³ g ⁻¹)	Meso= pore volume (BJH) (cm ³ g ⁻¹)	E ₀ (kJ mol ⁻¹)	n
Kiln	973	6		118.6							
		7	5.68	169.1	7	0.0067	0.0034	0.00462		11.714	4
Kiln	1073	2	6.26	199.1							
		3		293.5							
		4		380.3							
		5		378.0							
		6		399.4							
		7		443.2	321						

Table 4.2 (Continued)

Reactor	T (K)	HTt (h ⁻¹)	LHSV (cm ³ g h ⁻¹)	I ₂ number (mg I ₂ per gram carbon)	BET (m ² g ⁻¹)	V ₀ (t-Plot) (cm ³ g ⁻¹)	V ₀ (H-K) (cm ³ g ⁻¹)	V ₀ (DA) (cm ³ g ⁻¹)	Meso= pore volume (BJH) (cm ³ g ⁻¹)	E ₀ (kJ mol ⁻¹)	n
Kiln	1123	0.5	6.56	148.5							
		1	6.56	246.9							
		2		363.9							
		3		369.3	196.39	0.0776	0.0719	0.0873	0.0956	22.589	1.7
		4		401.9	239.70	0.0932	0.0869	0.1012	0.0957	22.232	1.9
		5		472.6	266.70	0.1015	0.0942	0.1108	0.1209	21.379	2.0
		6		418.8							
		7		448.7	276.89	0.0951	0.0945	0.1086	0.1031	21.160	2.1

Table 4.2 (Continued)

Reactor	T (K)	HTt (h ⁻¹)	LHSV (cm ³ g h ⁻¹)	I ₂ number (mg I ₂ per gram carbon)	BET (m ² g ⁻¹)	V ₀ (t-Plot) (cm ³ g ⁻¹)	V ₀ (H-K) (cm ³ g ⁻¹)	V ₀ (DA) (cm ³ g ⁻¹)	Meso= pore volume (BJH) (cm ³ g ⁻¹)	E ₀ (kJ mol ⁻¹)	n
Kiln	1173	2	6.85	283.4							
		3		294.6							
		4		297.8							
		5		256.7							
		6		306.5							
		7		318.6	190.13	0.0488	0.0614	0.0699	0.1157	19.852	2.4

Commercial product	I ₂ number (mg I ₂ per gram carbon)	Ash Content %	Moisture Content %
Soft drinks	1050		5 Maximum
NCP Chlookop	1000 - 1050	5 maximum	
Umgeni	600 - 1000	< 10	
Pharmaceuticals Manufacturing	1000	< 2	< 10
Alcoholic Beverages	> 400		

Table 4.3 Requirements of commercially activated carbons used

The data in Table 4.2 and Figure 4.1 show that the total surface area (as reflected by measured iodine numbers) increased with increasing heat treatment time and temperature. The total surface area levels over prolonged times ($t > 5$ hours) and the largest surface areas were obtained at $T = 1123$ K. Under the current experimental conditions the largest total surface area that was obtained in the fluidised bed was $524 \text{ m}^2 \text{ g}^{-1}$. According to total surface area specifications by South African activated carbon end users only Umgeni and the alcoholic beverages market sectors would be interested in an activated carbon with surface areas in this range. When the requirements for the ash and moisture content in Table 4.3 is compared with that of the Smartie coke as given in Table 4.1 the market would be much wider. Thus, during future efforts the focus will have to be to produce products with larger surface areas.

Statistical analysis was performed on the data collected from the experiments to determine the effect of temperature and heat treatment time on the iodine number. From the analysis, it was clear that there is a difference between the reactors as far as the iodine number is concerned.

A response surface analysis was performed on the data. The response surface of time and temperature is given in Figure 4.2. Looking at the response plot for temperature and time for the rotary kiln, it is clear that an optimum for the process variables exist. From the response surface plot for the FB it can be observed that temperature and time needs to be increased to increase the iodine number even further.

The resulting regression models for the rotary kiln and FB are given by Equations 4-1 and 4-2 respectively.

$$I_2 = -10756.726 + 26.385(HTT) - 0.0159(HTT)^2 + 73.544(HTt) - 5.706(HTt)^2 \quad (4-1)$$

$$I_2 = -4521.099 + 11.163(HTT) - 0.0066(HTT)^2 - 128.789(HTt) + 0.221(HTT)(HTt) \quad (4-2)$$

The models show the significant terms of temperature and time, which describes the response of iodine number. In the case of the model for the rotary kiln, temperature and time have significant linear and quadratic terms (p-value < 0.05). In the case of the model for the FB temperature and time have significant linear effects (p-value < 0.10). Only temperature has a significant quadratic effect and there is an interaction between temperature and time present. The models can be used to predict the iodine number for any combination of temperature and time within the experimental ranges. These numbers can however only be achieved at very high carbon conversion rates and it therefore becomes economically unviable. Green et al reached the same conclusions in their work⁵⁶ at the University of Kansas. It is therefore only cited as a theoretical value of what can be achieved.

If the regression models are used to predict the iodine number at the optimum conditions, the following results are obtained:

- Optimum conditions for the rotary kiln : The maximum iodine number occurs at a temperature of 829 K and a heat treatment time of 6.4 hours. The iodine

number at these conditions is 420.7 mg I₂ per gram carbon. The 95% confidence interval for the predicted value is [315.2; 526.2].

- Optimum conditions for the FB : The maximum iodine number will occur beyond the experimental ranges. The prediction of the iodine number is 711.0 mg I₂ per gram carbon at a temperature of 900 K and a heat treatment time of 7 hours. The 95% confidence interval of the prediction is [513.66; 908.38].

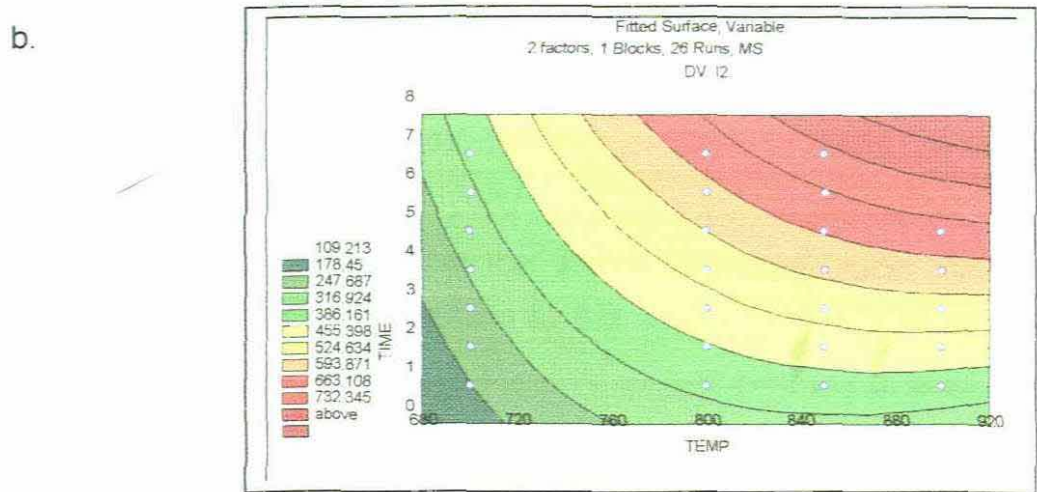
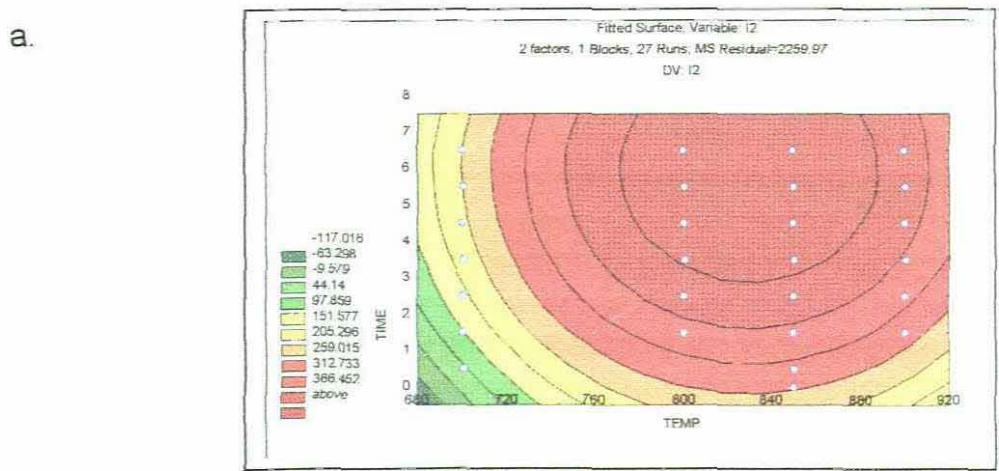


Figure 4.2 Response surface of time and temperature. a. Rotary kiln. b. FB.

In the case of the FB the experiments in Table 4.4 can be followed for temperature and time in order to try and improve the iodine number. When the iodine number does not increase anymore an experimental design program

should be deployed to determine the effects of temperature and time at that stage.

Experiment	Step size		Experimental conditions		Predicted iodine number/mg iodine per gram carbon
	Temp/K	Time/h	Temp/K	Time/h	
			900	5	570
1	100	3.70	1000	8.7	895
2	200	7.40	1100	12.4	1252
3	300	11.1	1200	16.1	1642
4	400	14.8	1300	19.8	2065
5	500	18.5	1400	23.5	2520

Table 4.4 Proposed additional activation trials for the FB reactor

It is possible to calculate the percentage carbon conversion from the activation trials in the rotary kiln. These values can then be used in Equation (2) (Table 3.1) to calculate the reactivity at each carbon conversion. The reactivities are plotted as function of carbon conversion in Figure 4.3. The data in Figure 4.3 show that in general low carbon conversions were obtained in the rotary kiln. The reactivities increase as function of time. There are two possible explanations for this phenomenon:

In the first place is it possible that the random pore model can describe the gasification reaction⁵⁷. According to this model there is an initial increase in reactivity due to an increase in the total surface area but at later stages of the reaction the process of random overlapping of pore surfaces reduces the area available for reaction. Thus in correspondence with this model at some stage of the gasification reaction the reactivities would start to decline again.

Alternatively is it possible that the gasification reaction proceeds according to a shrinking core model. According to this model the iron present in the coke will affect the gasification rate profile. In non-catalytic gasification reactions, the rate

will not change significantly with conversion. In catalytic gasification reactions, the rate will steadily increase with conversion, and it will decrease at higher carbon conversion levels. The increase in reactivity with increasing carbon conversion in the case of the catalyzed reactions could be due to an increase in the metal cation concentration at the external surface of small non-porous grains (particle constituents) with increasing burn-off. At higher carbon conversion a decrease in the gasification rate will be observed due to a collapse of the particle structure, pore plugging, metal loss due to migration of iron into the pores⁵⁸ or iron sintering.

To further investigate the matter a kinetic analysis of the carbon gasification rate was performed by fitting the experimental carbon conversions to the random pore and shrinking core models (Table 3.1). The experimental carbon conversions and the fitted curves are shown in Figure 4.4 and in general a good agreement between the experimental and theoretical values were obtained. Consequently it can be deduced that both of these models describe the experimental carbon conversions well and it is possible that under the present conditions the “end stages” of the models under investigation have not been reached. This is supported by the fact that the reactivities in Figure 4.3 have not reached an optimum value and it can be deduced that it is possible to obtain larger surface areas if the heat treatment time is further increased. Thus, under the current experimental conditions, the inherent reactivity of the precursor does not limit the development of the total surface area. These observations are supported by the statistical treatment of the data.

Based on the evidence at hand it is difficult to conclude on the applicability of the two models for the gasification of the “Smartie” coke. But, since there is iron in the “Smartie” coke sample it is expected that the shrinking core model is describing the gasification process at least partially. This proposition is reinforced by the fact that it is more difficult to activate the green MTP coke, which does not contain any iron, than the green “Smartie” coke. It should be kept in mind that other precursor characteristics such as the porosity, degree of

graphitisation and surface oxygen functional groups also have an influence on the pore structure development. It is therefore dangerous to ascribe differences in activation between the green MTP and "Smartie" coke precursors solely due to the difference in their respective iron contents.

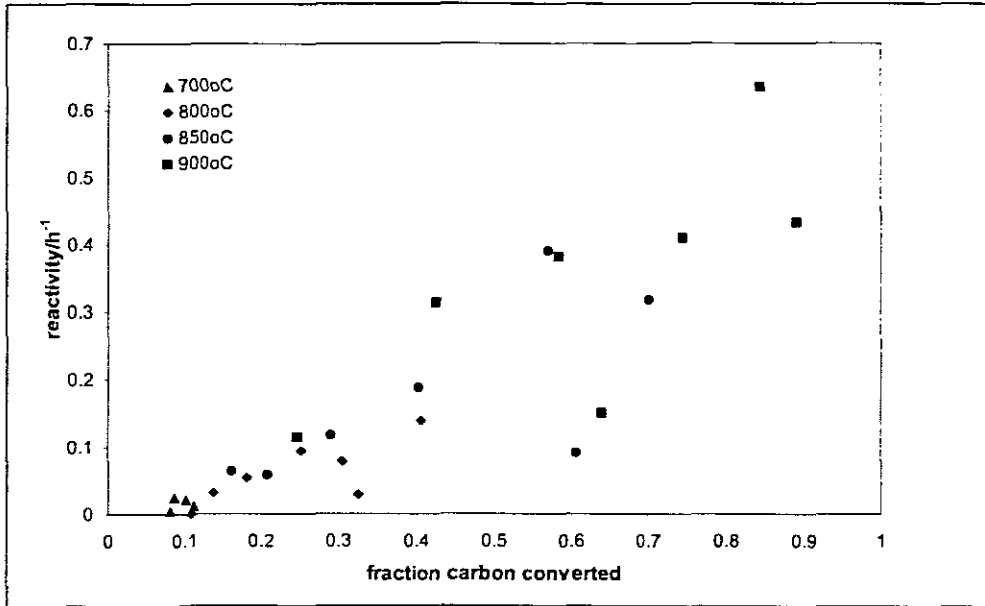


Figure 4.3 Reactivity as function of carbon conversion.

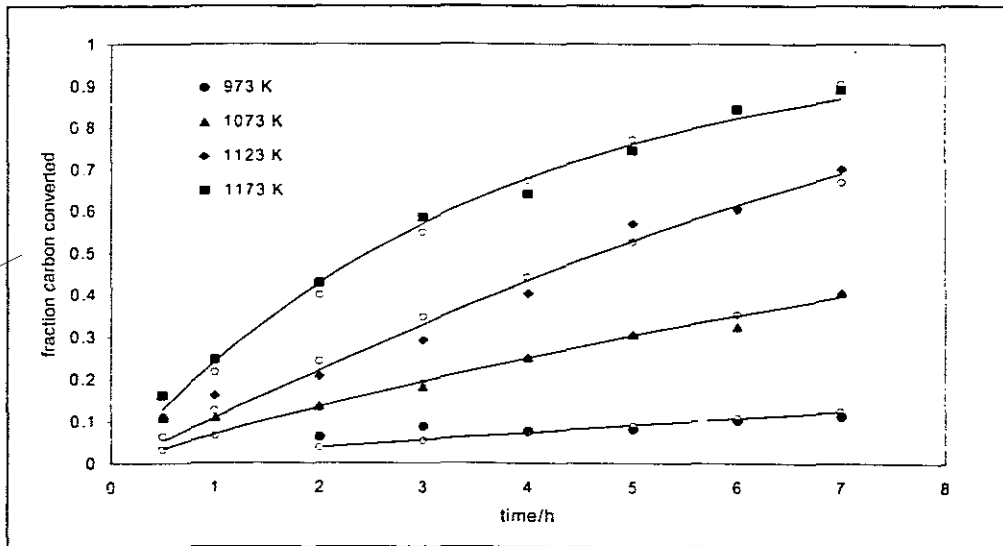


Figure 4.4 Carbon conversion as function of time.

The solid lines and open circles are theoretical values calculated from a non-linear regression fit of the experimental carbon conversions to the random pore and shrinking core models respectively.

CHAPTER 5

CARBON CHARACTERISATION

SUMMARY

In order to evaluate the activated carbons in more detail some of their adsorption isotherms were determined. This adsorption data can also be employed to determine the pore size distributions of the activated carbons.

Adsorption in "Smartie" coke derived activated carbon

The *adsorption isotherms* for the activated carbons produced in the FB and rotary kiln at 3 different temperatures are given in Figures 5.1 to 5.3. Although the shape of the isotherms changes as function of temperature they all appear to be of Type IV in the BDDT classification, which are normally obtained for carbons with micro- and mesopores. The products obtained at the lower temperatures have a more microporous structure than the products obtained at the higher temperatures.

The open loop hysteresis that was sometimes observed (especially evident for the products obtained in the FB at 973 K) indicates that the equilibrium time allowed for desorption was too short. This phenomenon generally is observed in the case when emptying a pore filled with nitrogen occurs at a lower pressure than the filling of the pore due to constrictions in the pore, for example a narrow pore entrance. Typically these pores can be bottleneck shaped.

It can be concluded that the shape of the hysteresis could suggest that the activated carbons contain mesopores with an upper size restriction and the products activated at the lower HHT and HHT exhibit the highest degree of microporosity (see also discussion later on). The increasing degree of hysteresis

with increasing temperature suggests that the mesoporosity also increases with increasing temperature.

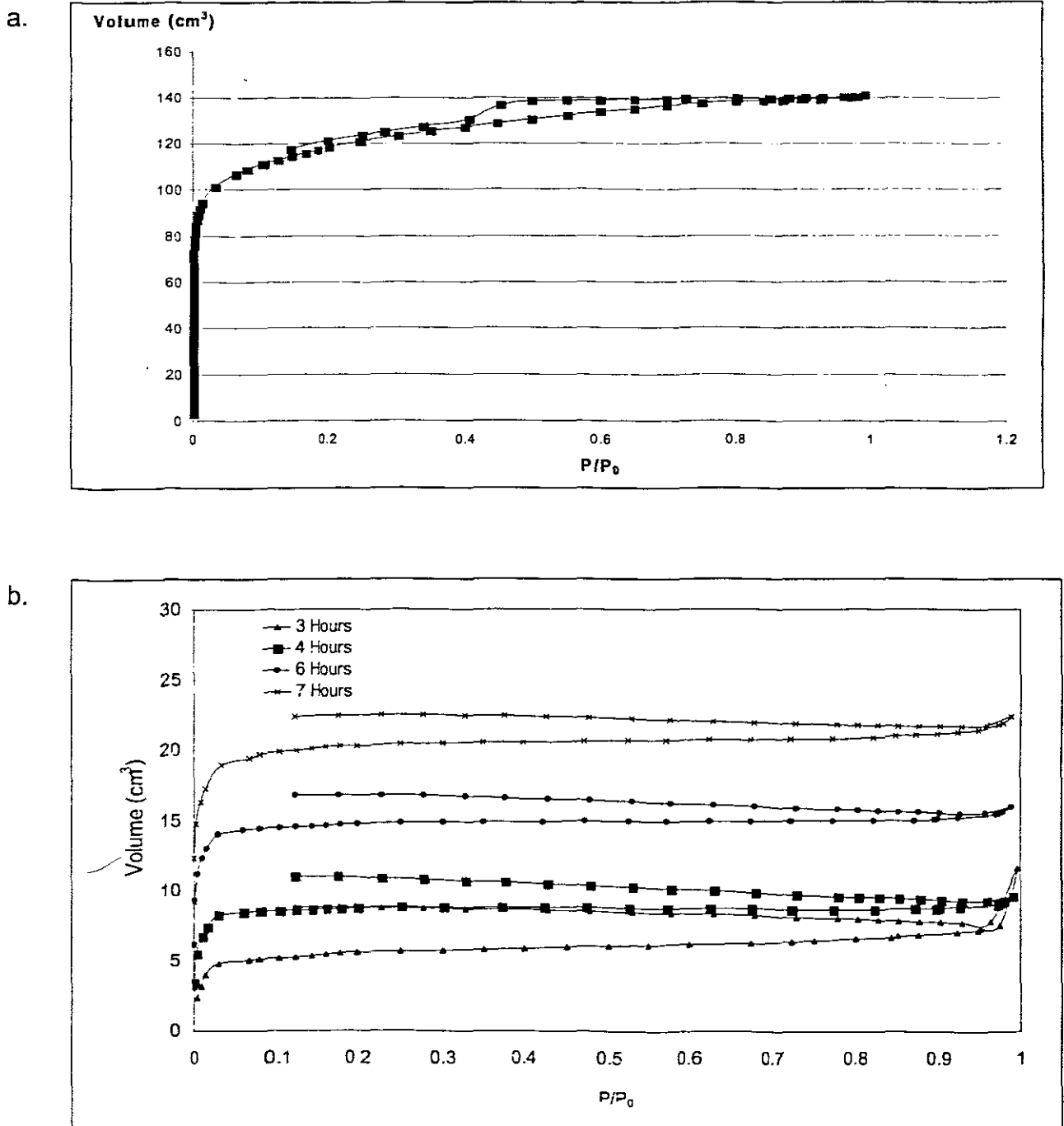


Figure 5.1 Adsorption-isotherm of N_2 by "Smartie" coke derived activated carbon. a. activation in the rotary kiln (experimental conditions : steam LHSV = $5.68 \text{ cm}^3 \text{ g}^{-1} \text{ h}^{-1}$; $T = 973 \text{ K}$; HTt = 7 hours). b. activation in the FB (experimental conditions : steam LHSV = $61.7 \text{ cm}^3 \text{ g}^{-1} \text{ h}^{-1}$; $T = 973 \text{ K}$).

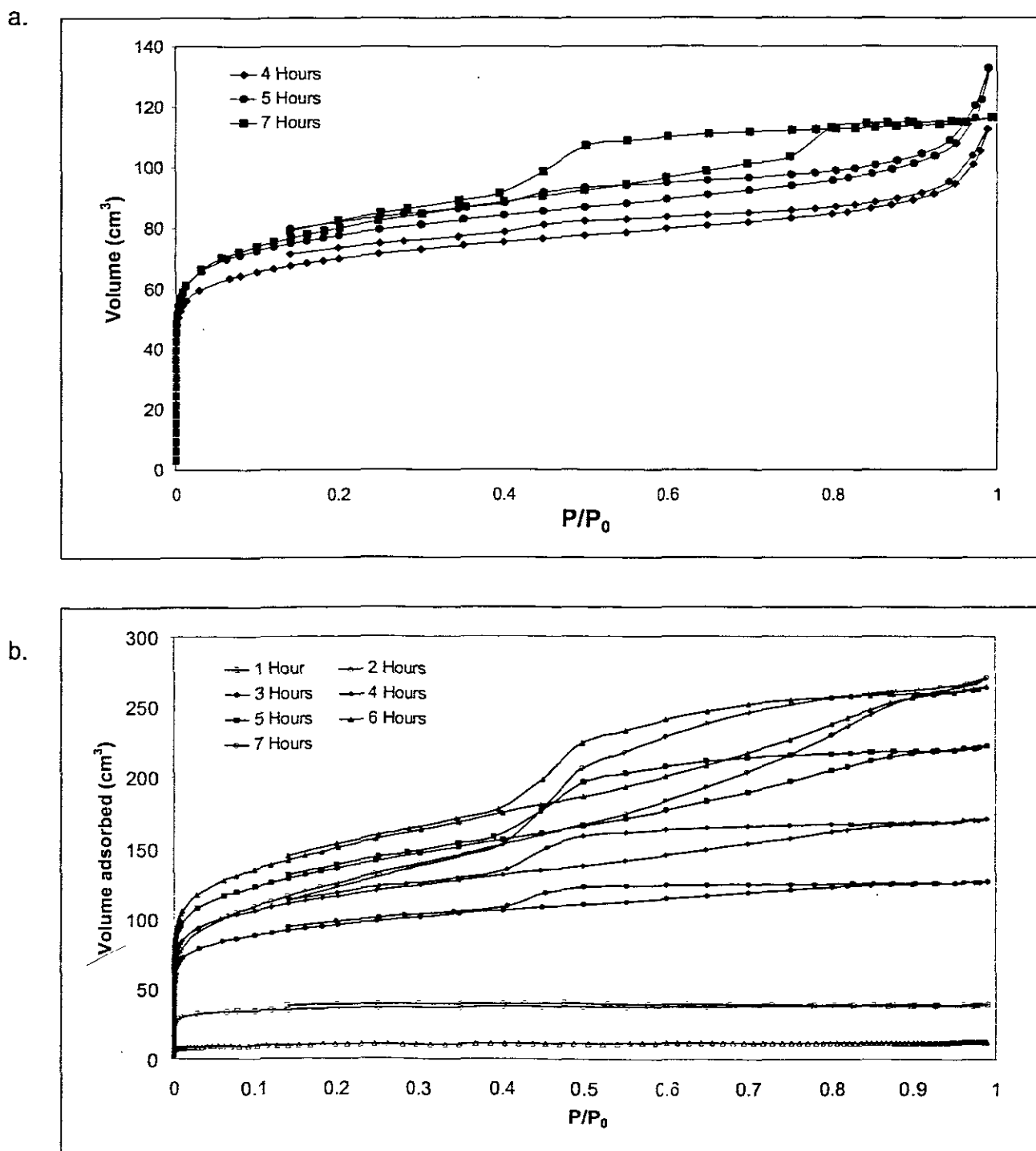


Figure 5.2 Adsorption-isotherm of N_2 by "Smartie" coke derived activated carbon. a. activation in the rotary kiln (experimental conditions : steam LHSV = $6.56 \text{ cm}^3 \text{ g h}^{-1}$; $T = 1123 \text{ K}$). b. activation in the FB (experimental conditions : steam LHSV = $71.0 \text{ cm}^3 \text{ g h}^{-1}$; $T = 1123 \text{ K}$).

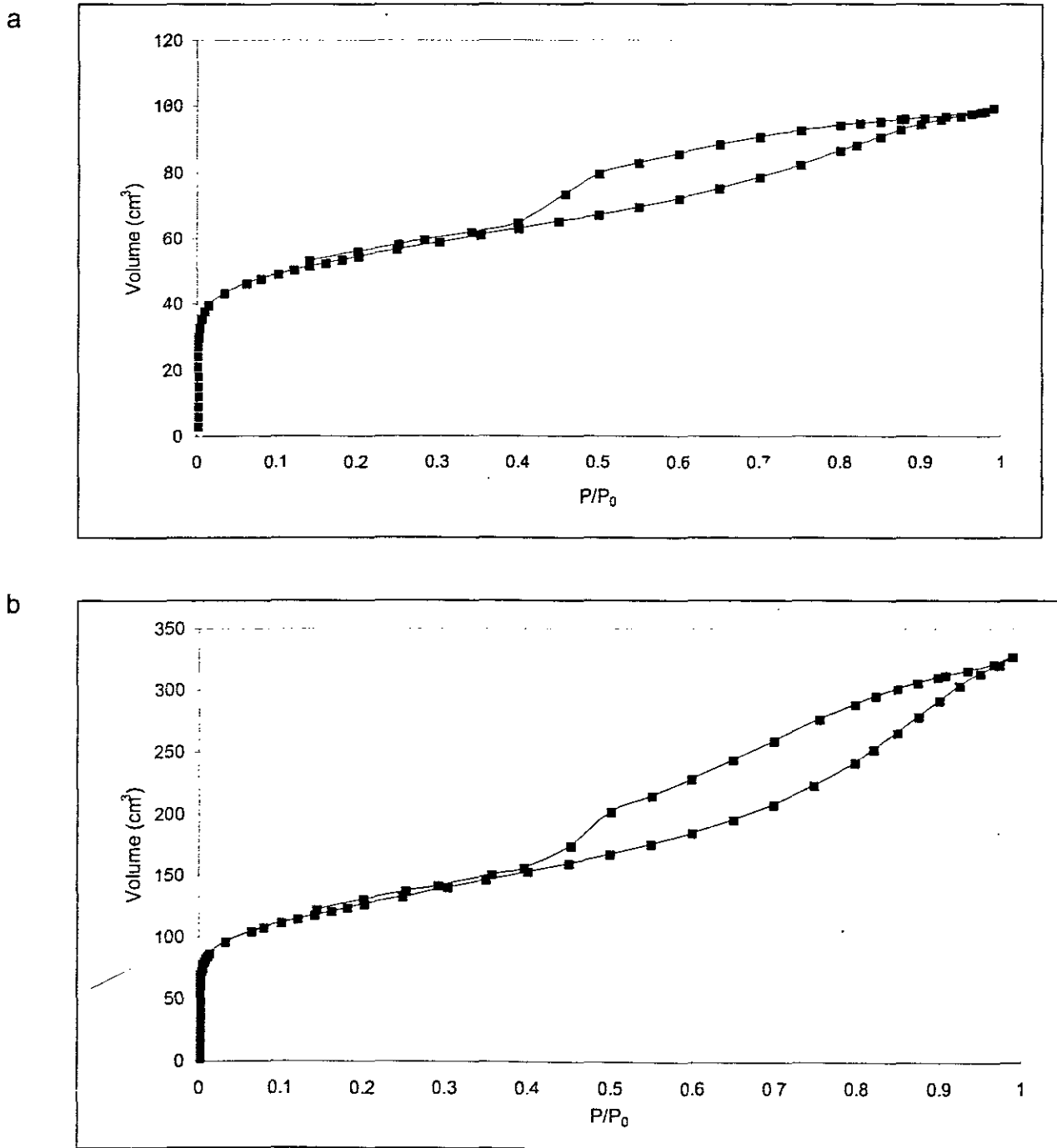


Figure 5.3 Adsorption-isotherm of N_2 by "Smartie" coke derived activated carbon. a. activation in the rotary kiln (experimental conditions : LHSV = $6.85 \text{ cm}^3 \text{ g}^{-1} \text{ h}^{-1}$; $T = 1173 \text{ K}$; HTt = 7 hours). b. activation in the FB (experimental conditions : LHSV = $74.3 \text{ cm}^3 \text{ g}^{-1} \text{ h}^{-1}$; $T = 1173 \text{ K}$; HTt = 4 hours).

To evaluate the *surface characteristic energy*, E_0 , *structural heterogeneity parameter*, n , and *limiting micropore volume*, V_0 , the experimental values of V_{ads} were fitted to the DA equation (equations 2-7 and 2-9). The values for E_0 , n and V_0 are also given in Table 4.2.

It is evident from these results that the values of E_0 increases with increasing HTT up to a distinct maximum after which it declines again. In general, an adsorbate-adsorbent system of low E_0 has a more homogeneous microporous structure than a system of a high E_0 value. Also, a small value of n denotes a heterogeneous micropore structure with a broad micropore size distribution; while a large value denotes the opposite. The value of n approaches 3 only for some activated carbons with particularly uniform microporosity. Based on this evidence; it is anticipated that the microporosity of the different activated carbons given in Table 4.2 would increase with decreasing temperature. Although the mesoporosity increases with increasing HTT and HTt the values of n suggest that a uniform micropore distribution would be obtained at higher carbon conversions. Also, if one compares the data at 1173 K the products activated in the rotary kiln, will have a more heterogeneous micropore structure than the products from the FB.

Important to note is the influence of the heat treatment temperature and heat treatment time on the development of the micropore volume (Figures 5.4 & 5.5). A distinct maximum is observed that is higher for higher activation temperatures. Low temperature activation exhibits a rapid increase of the micropore volume up to approximately 6 hours HTt, possibly due to opening of restricted pores, whereas further burning off results only in minor changes in the micropore volume. In the case of activation in the FB the mesopore development on the other hand exhibits a steady course.

It can be concluded that low activation temperatures and treatment times lead to more microporous carbons than high activation temperatures.

It is possible to accurately predict isotherms utilizing the DFT theory. Generally, the DFT predictions compare well with simulation results using Monte Carlo or molecular dynamics. Therefore the DFT theory was utilised to calculate the integral pore size distributions for the different samples. These calculations result in pictorial displays of the pore size distributions over the complete range of the isotherm; and reinforce the deductions from the information in Figures 5.1 to 5.3 and Table 4.2.

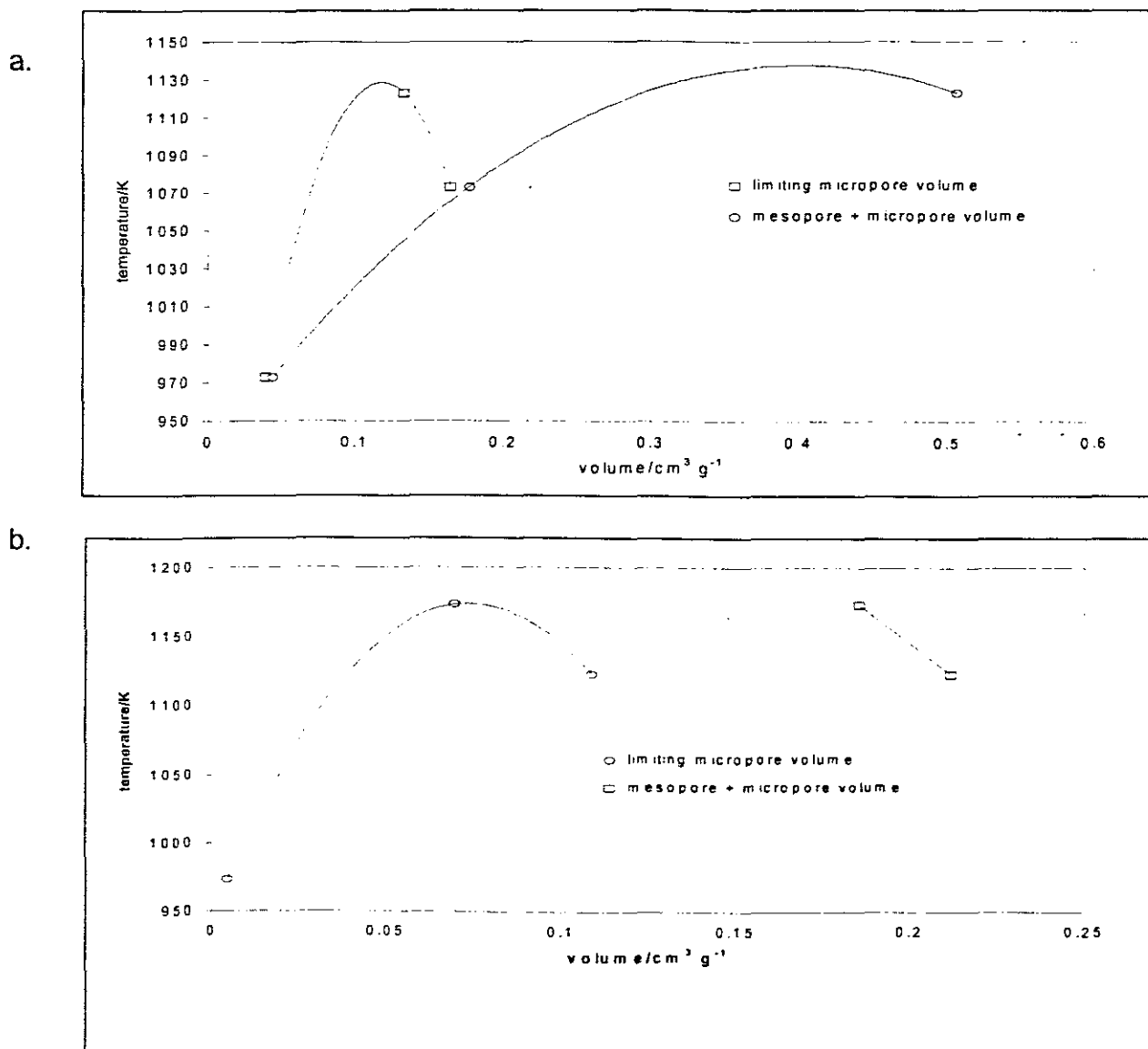


Figure 5.4 Micropore and micropore+mesopore volume per unit weight starting material as function of HTT a. activation in FB b. activation in rotary kiln.

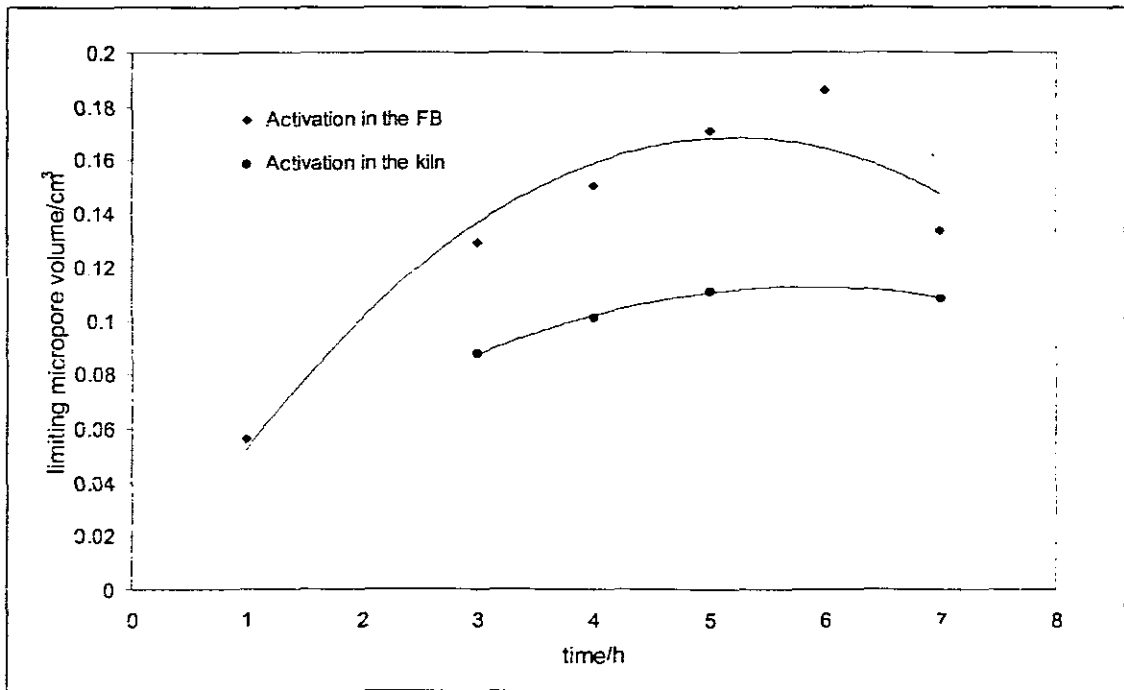


Figure 5.5 Micropore volume per unit weight starting material as function of HTt

The pore size distributions as a function of heat treatment time and temperature are given in Fig.'s 5.6 to 5.10. In general they underline the findings from the isotherms:

- In correspondence with the isotherms the products obtained at 973 K are predominantly microporous. If the temperature is increased the porosity shifts to a pore structure that has also a well-developed mesoporous structure.
- The mesoporosity increases with increasing HTt.
- When comparing the pore size distributions at 1123 K of the products from the rotary kiln with that of the products from the FB both show a well-developed mesopore distribution with the activated carbon in the kiln also indicating a macropore distribution.
- Slightly higher surface areas could be obtained upon activation in the fluidised bed when compared to that at the same temperatures in the rotary kiln. In

general, this implies that this precursor can be activated in either the rotary kiln or the fluidised bed.

- At 1123 K the bulk of the pore size is in the range of 20 - 200 Angstroms and, as mentioned earlier, this is according to the IUPAC classification of pore sizes seen as mesopores.

One can conclude that the activated carbon produced from "Smartie" coke will be suitable for the treatment of waste water.

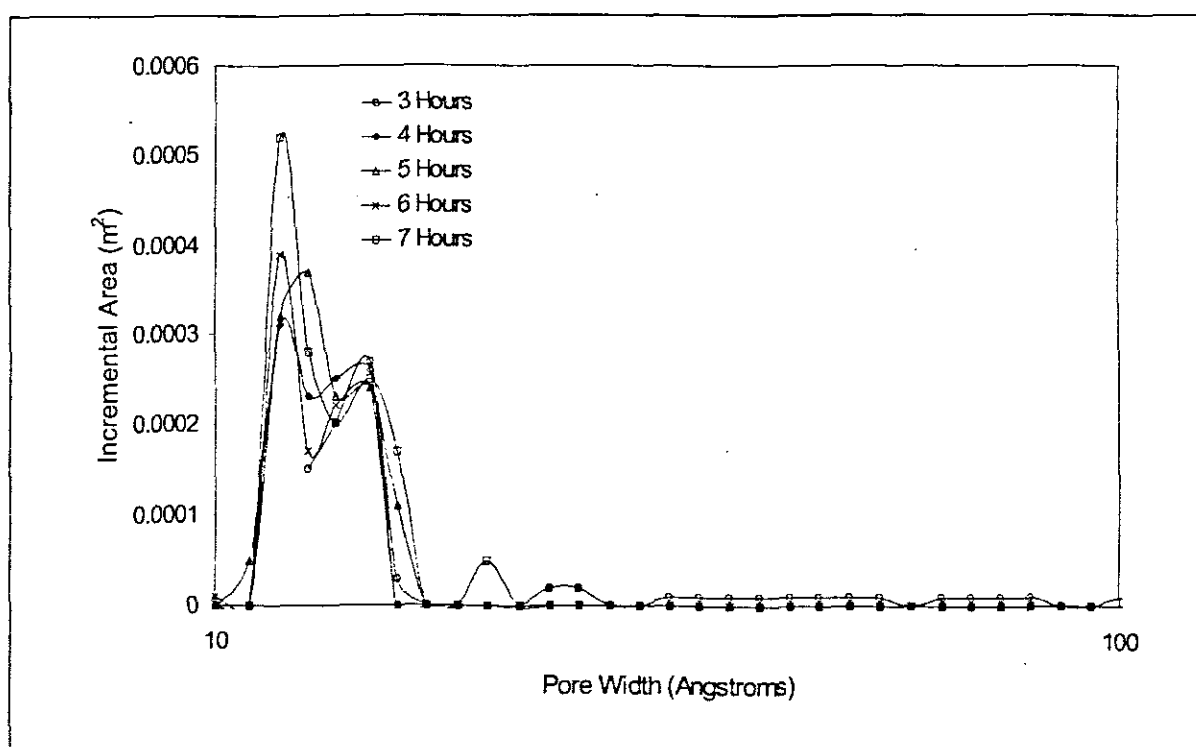


Figure 5.6 Pore size distribution of the activated carbons produced in the FB. Experimental conditions: $T = 973 \text{ K}$; $\text{LHSV} = 61.7 \text{ cm}^3 \text{ g}^{-1} \text{ h}^{-1}$.

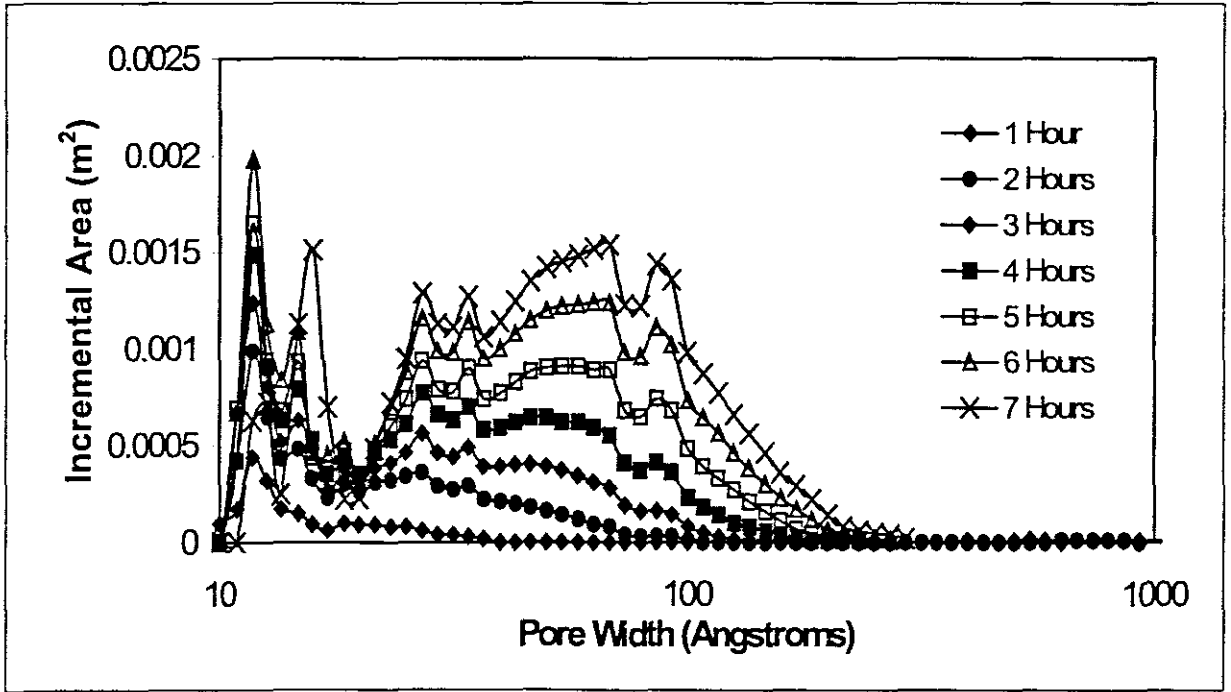


Figure 5.7 Pore size distribution of the activated carbon produced in the FB. Experimental conditions: $T = 1123 \text{ K}$; $\text{LHSV} = 71.0 \text{ cm}^3 \text{ g}^{-1} \text{ h}^{-1}$.

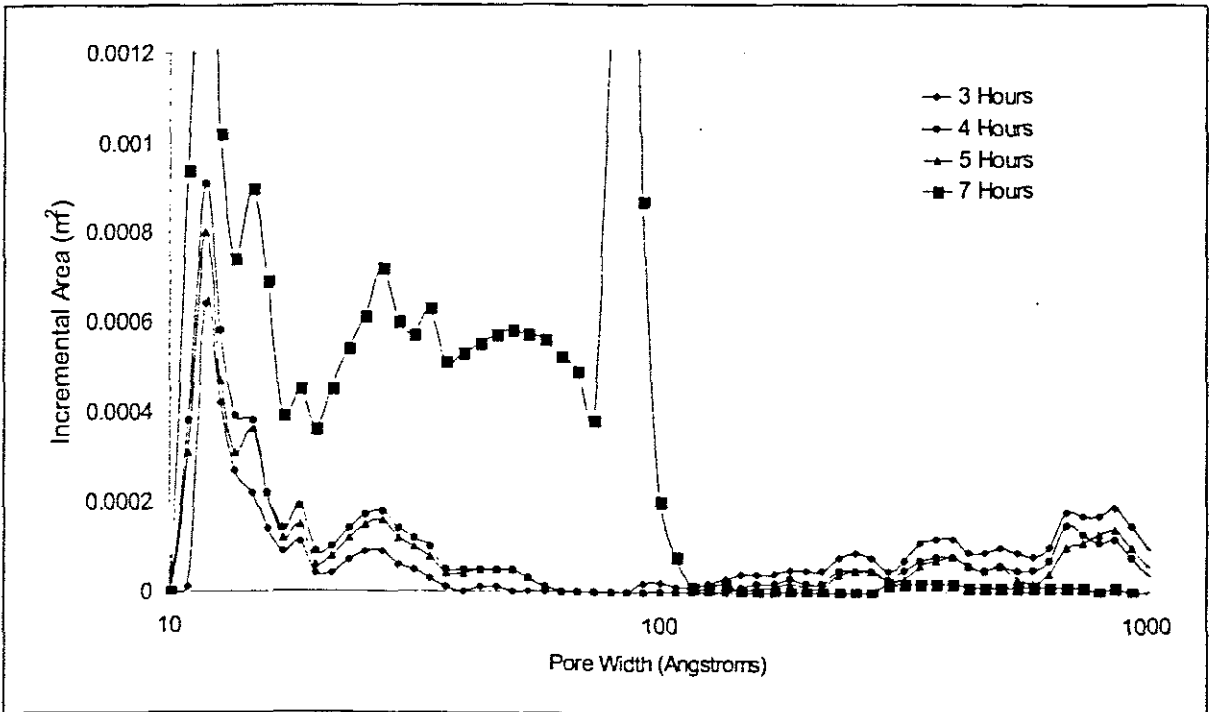


Figure 5.8 Pore size distribution of the activated carbon produced in the rotary kiln. Experimental conditions: $T = 1123 \text{ K}$; $\text{LHSV} = 6.56 \text{ cm}^3 \text{ g}^{-1} \text{ h}^{-1}$.

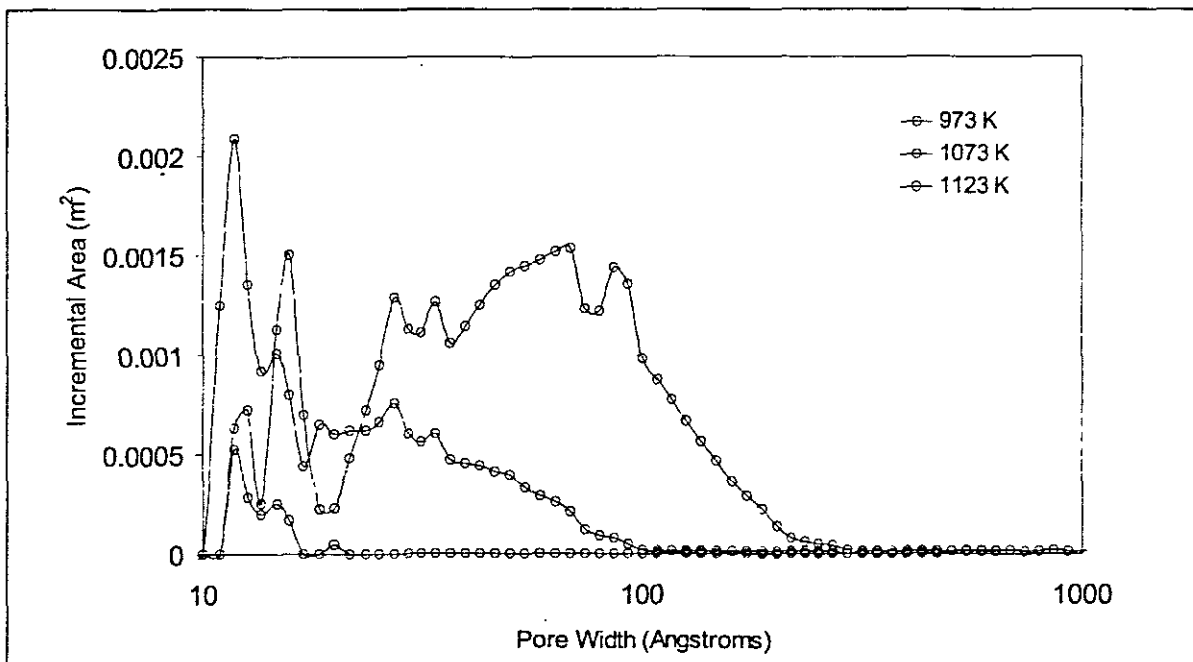


Figure 5.9 Pore size distribution of activated carbons produced in the FB. HTt = 7 hours.

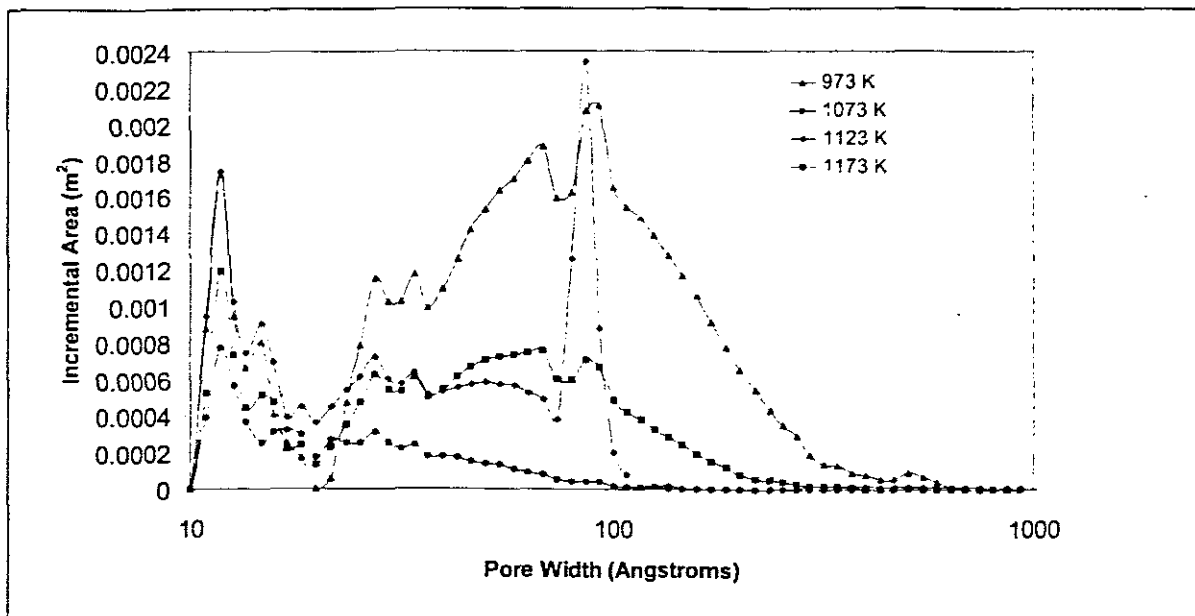


Figure 5.10 Pore size distribution of activated carbons produced in the rotary kiln. Experimental conditions: HTt = 7 hours.

The information from the adsorption data is important because it shows that it will be possible to produce virtually any product within the specification of a potential client. For example during a discussion with Umgeni Water Board during 1998 it became evident that an important criterion for activated carbon for water treatment is its geosmin adsorption capacity. Molecular graphics of the geosmin molecule showed that it is relatively small; with a maximum and minimum diameter of 7.3 Å and 5.43 Å respectively. Accordingly it is possible that the geosmin molecule could fit into the split shaped micropores of the activated carbons, and a small micropore distribution would be beneficial for the adsorption of the geosmin molecule. The total surface area must thus be interpreted together with the pore distribution in order to predict an activated carbons geosmin adsorption capacity.

CHAPTER 6

CARBON ADSORPTION TESTS

SUMMARY

In order to evaluate the adsorption capabilities of the manufactured activated carbon it was first tested for its gold adsorption potential. This was followed by a study for the possible use in the water purification market. The results of these tests will be discussed in the following chapter

6. Adsorption of gold cyanide onto activated carbon

In order to evaluate the Smartie coke activated carbon it was tested for its $\text{Au}(\text{CN})_2^-$ adsorption potential against a commercial activated carbon (ANK) that is currently in use in the CIP process.

6.1 Calculation of the rate constant

As discussed earlier (see section 2.9) the rate constants can be calculated from the equation $\ln[\text{Au}] = \ln[\text{Au}]_0 - kt$.

The values of $[\text{Au}]$ and $[\text{Au}]_0$ as well as the rate constants for the various tests are given in Tables 6.1 – 6.4.

pH	[Au] t = 30 min (Smartie) (g/l)	[Au] t = 0 (Smartie) (g/l)	[Au] t = 30 min (ANK) (g/l)	[Au] t = 0 (ANK) (g/l)	k (Smartie) (min ⁻¹)	k (ANK) (min ⁻¹)
11.44	18.42	21.84	19.38	21.77	3.71×10^{-3}	3.07×10^{-3}
10	18.05	19.22	20.03	20.24	1.87×10^{-3}	2.77×10^{-4}
6.46	17.78	20.82	18.22	20.65	2.34×10^{-3}	2.23×10^{-3}

Table 6.1 Calculated rate constant for adsorption with pH varied. $[Au_0] \sim 20$ ppm

pH	[Au] t = 30 min (Smartie) (g/l)	[Au] t = 0 (Smartie) (g/l)	[Au] t = 30 min (ANK) (g/l)	[Au] t = 0 (ANK) (g/l)	k (Smartie) (min ⁻¹)	k (ANK) (min ⁻¹)
9.8	35.18	40.84	37.25	40.56	3.86×10^{-3}	2.24×10^{-3}
10	18.05	19.22	20.03	20.24	1.87×10^{-3}	2.77×10^{-4}
10.06	8.46	11.2	9.89	11.04	9.60×10^{-3}	3.05×10^{-3}

Table 6.2 Calculated rate constant for adsorption with $[Au_0]$ varied. pH ~ 10

Mass (g)	[Au] t = 30 min (Smartie) (g/l)	[Au] t = 0 (Smartie) (g/l)	[Au] t = 30 min (ANK) (g/l)	[Au] t = 0 (ANK) (g/l)	k (Smartie) (min ⁻¹)	k (ANK) (min ⁻¹)
0.2	18.05	19.22	20.03	20.24	1.87×10^{-3}	2.77×10^{-4}
0.5	12.13	20.47	18.79	20.30	1.52×10^{-2}	2.14×10^{-3}

Table 6.3 Calculated rate constant for adsorption with mass of activated carbon used varied: pH ~ 10 , $[Au_0] \sim 20$ ppm

Environ= ment	[Au] t = 30 min (Smartie) (g/l)	[Au] t = 0 (Smartie) (g/l)	[Au] t = 30 min (ANK) (g/l)	[Au] t = 0 (ANK) (g/l)	k (Smartie) (min ⁻¹)	k (ANK) (min ⁻¹)
O ₂	18.05	19.22	20.03	20.24	1.87 x 10 ⁻³	2.77 x 10 ⁻⁴
N ₂	18.16	19.18	19.88	20.14	1.38 x 10 ⁻³	7.90 x 10 ⁻⁵

Table 6.4 Calculated rate constant for adsorption with adsorption environment varied. pH ~ 10, [Au₀] ~ 20 ppm

6.2 Influence of operating parameters

Comparative tests were done under various conditions. These include different pH conditions, gold concentrations, the adsorbing environment as well as the amount of activated carbon used for adsorption. The results of these are given in Figures 6.1 to 6.4

6.2.1 Effect of pH on gold adsorption

Although the initial experimental data are scattered, Figure 6.1 shows that the lower the pH of the solution the higher the capacity for gold on the carbon. There was no distinct difference in the equilibrium concentrations of the higher pH samples. In the case of ANK, an increase in pH resulted in an increase in the value of k. No independent relation between k and pH could be obtained for Smartie Coke.

6.2.2 Effect of initial concentration on gold adsorption

The initial gold concentration is not suppose to affect the rate of adsorption. However, as can be seen in Table 6.2 it was impossible experimentally to obtain constant values for k at the different initial gold concentrations.

6.2.3 Effect of mass of carbon used on adsorption of gold

As was to be expected the batch in which 0.5 g of activated carbon was used, adsorbed more gold than did the batch with 0.2 g. This can be attributed to the fact that the 0.5 g batch would have a larger total surface area for adsorption. The 0.5 g batch has an adsorption rate (k) of 9 times faster than the 0.2 g batch. This is due to the faster driving force presented by the larger surface area.

6.2.4 Effect of environment of adsorption

From Figure 6.4 it can be seen that the adsorption capacity in an O_2 environment is higher than for a nitrogen environment.

The initial gold concentrations were very similar. Due to the fact that the initial gold concentration determines the rate of adsorption, it was expected that the rates of adsorption (as can be seen from Table 6.4) should be fairly similar.

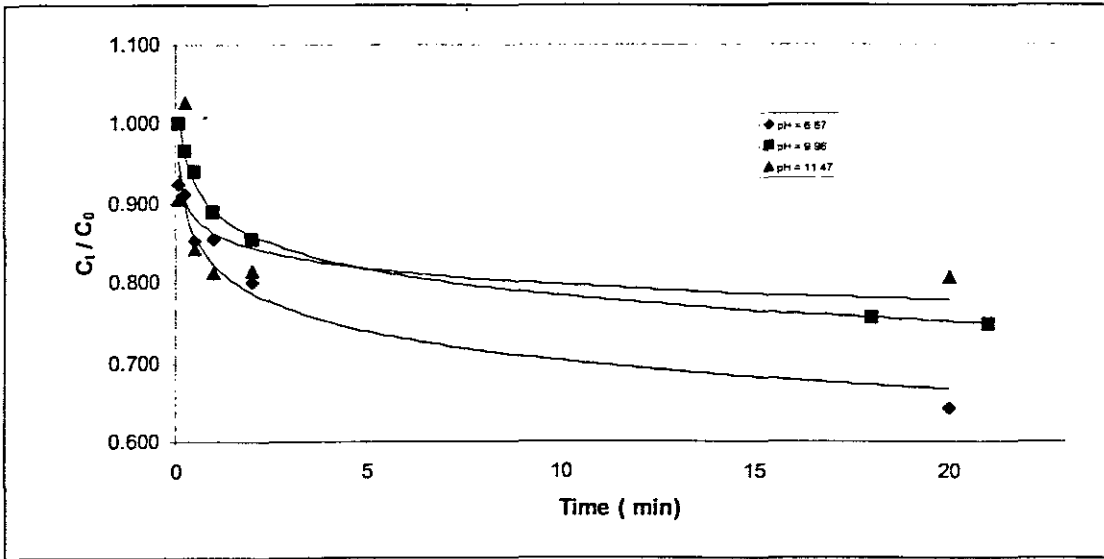


Figure 6.1 Adsorption tests at varying pH levels. [Au₀] ~ 20ppm, M = 0.2g, N = 200 rpm

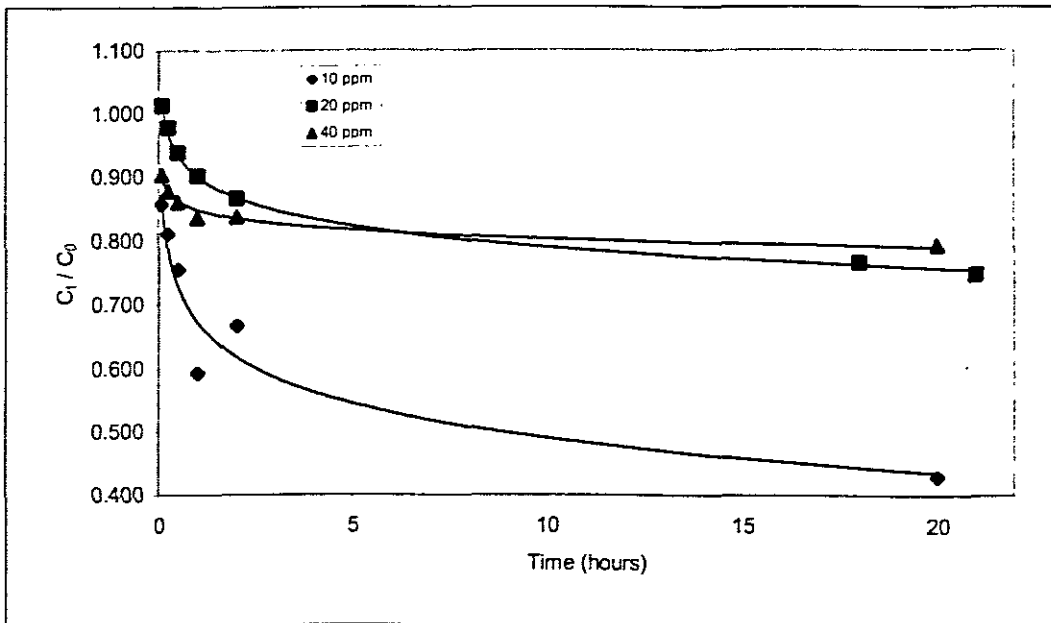


Figure 6.2 Adsorption tests at varying concentration levels. pH ~ 10, M = 0.2g, N = 200 rpm

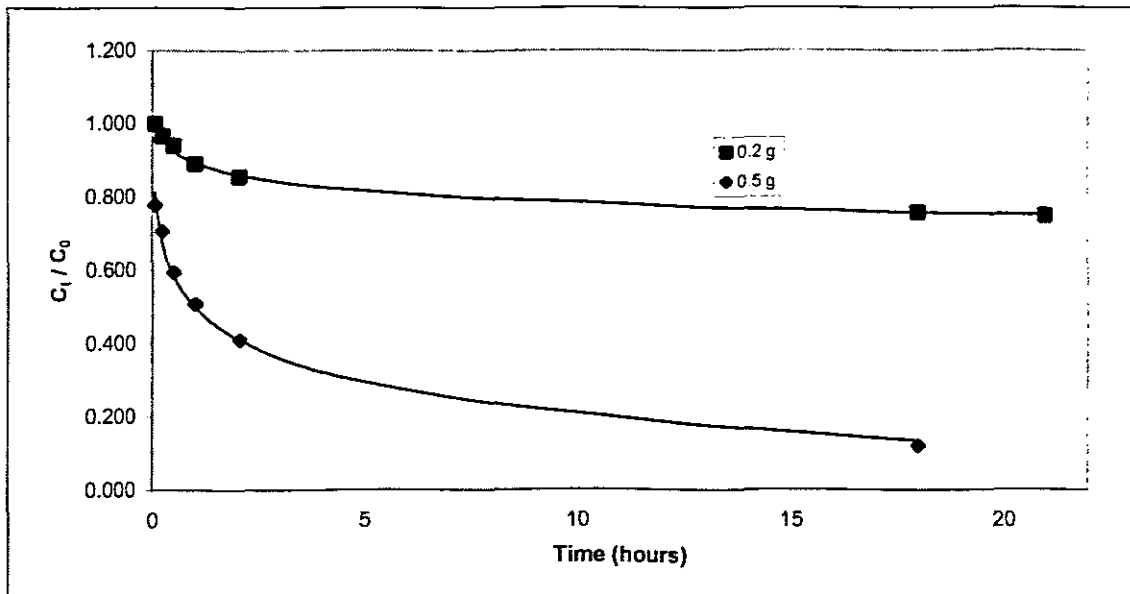


Figure 6.3 Adsorption tests at varying mass of activated carbon used pH ~ 10, $[Au_0] \sim 20\text{ppm}$, $N = 200\text{ rpm}$

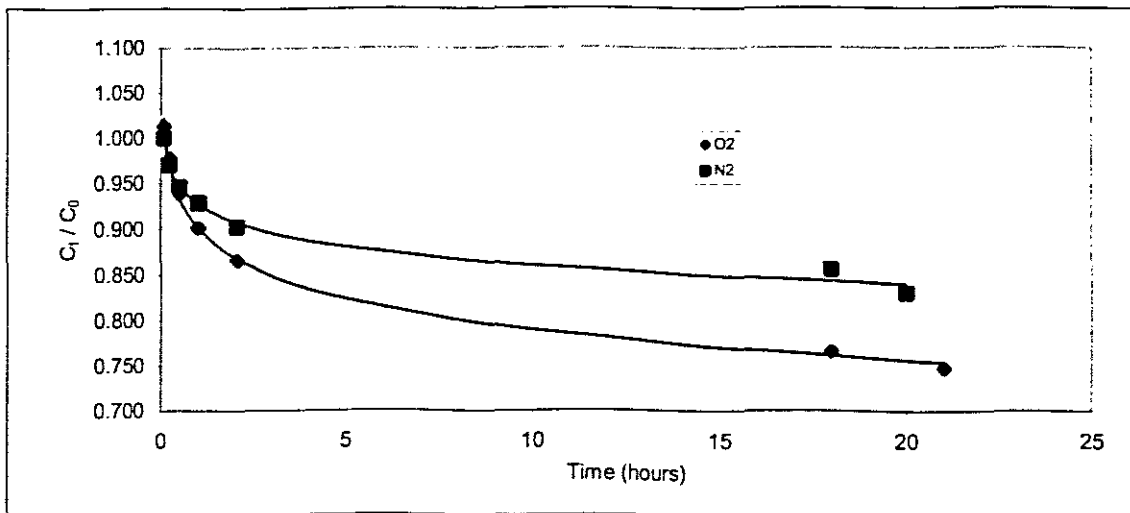


Figure 6.4 Calculated rate constant for adsorption with adsorption environment varied. pH ~ 10, $[Au_0] \sim 20\text{ ppm}$, $M = 0.2\text{g}$, $N = 200\text{ rpm}$

6.3 Comparative study

In order to evaluate the effectiveness of the Smartie coke activated carbon in terms of its gold adsorption properties it was compared under similar conditions to ANK.

It can be seen from Figure 6.5 that not only did the smartie coke activated carbon compare well with the ANK, but it even outperformed ANK. Not only did it outperform as far as the adsorption rate was concerned but also as far as the equilibrium concentration is concerned. After 21 hours of adsorption the concentration in the solution with the smartie coke activated carbon was 1.5 ppm less than for that of the ANK.

It can then be concluded that even though the total surface area for the smartie coke carbon is considerably less than for the ANK it still compares well from an adsorption point of view.

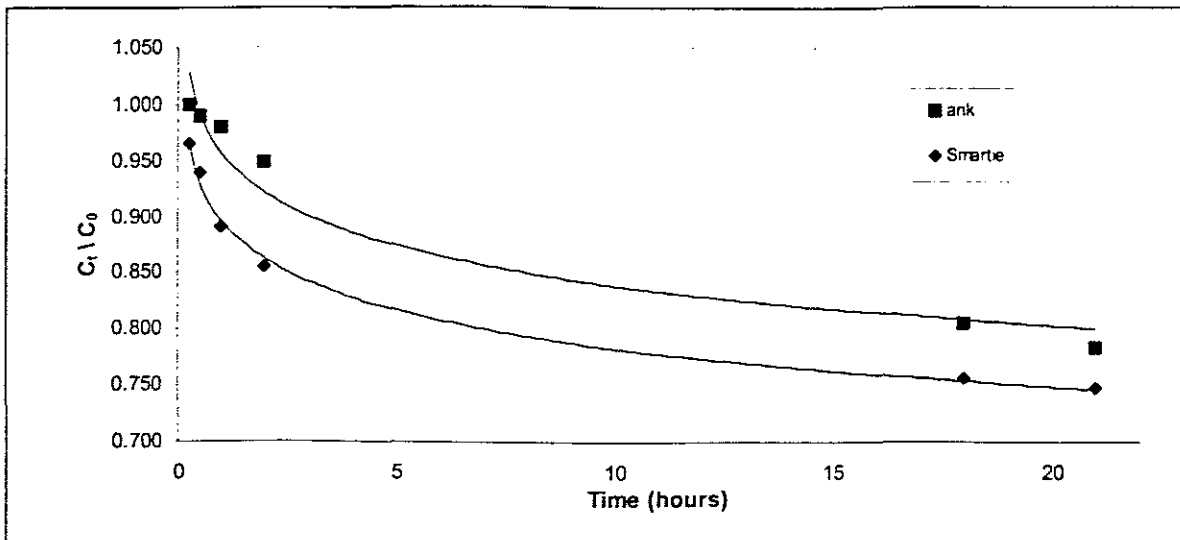


Figure 6.5 Comparison between gold adsorption of Smartie coke and ANK pH ~ 10, [Au₀] ~ 20 ppm, M = 0.2g, N = 200 rpm

6.4 Water Purification

As the water purification market is an alternative to the gold industry, the capabilities of the smartie coke for water treatment was also analysed. The

characteristics of the two test carbons are given in Table 6.5. From this table it can be seen that the Smartie coke compares well as far as the moisture content is concerned; however, the iodine number was very much lower.

The DOC level (dissolved organic content) of water is an indication of the amount of organic matter in the water. As the Smartie coke has such large pore size distributions it would favour the adsorption of the larger molecules.

In Figure 6.6 it can be seen that the smartie coke activated carbon had an initial adsorption of the dissolved organics equivalent to that of the activated carbon currently in use in the industry. This could be due to the large pore size distribution of the activated carbon. After six hours, however the quantity adsorbed started to decrease again with the smartie coke sample. This premature decrease of the adsorption in the case of the Smartie coke could be due to the influence of the functional groups present in the Smartie coke. This would then be an indication of a distinct difference in the composition of the functional groups of the two activated carbons used in the test.

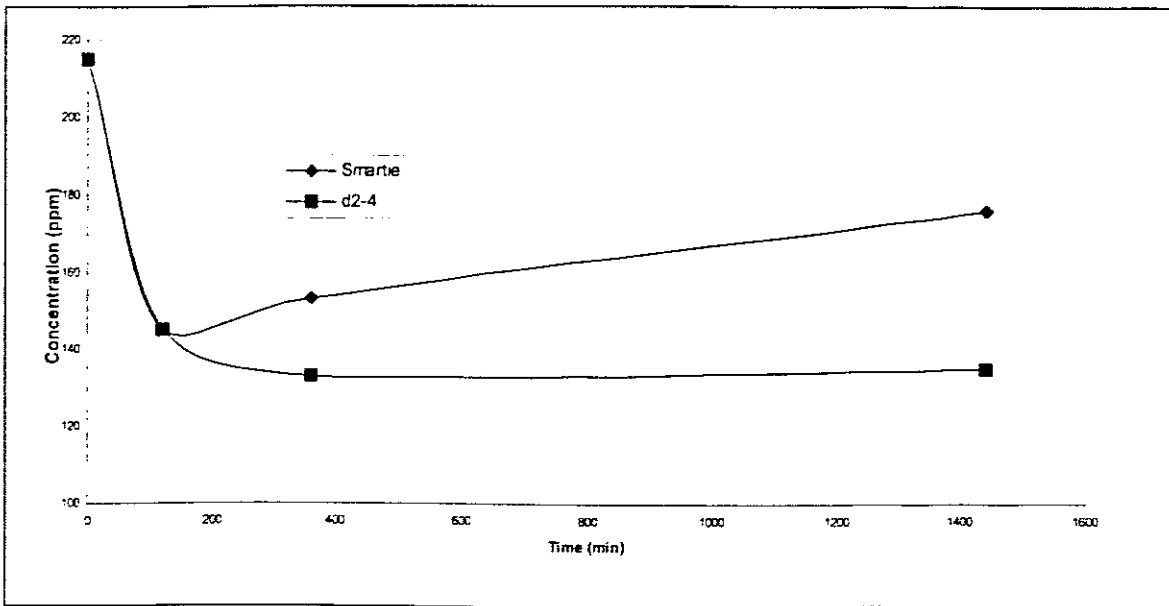


Fig 6.6 DOC results of the two test carbons

Name	Particle size (mm)	Carbon source	Moisture %	Iodine nr
3 ml	1.0 - 2.36	Smartie Coke	1	576
D2-4	1.0 - 3.0	Wood	> 10	1000

Table 6.5 Characteristics of the test carbons for water purification

CHAPTER 7

CONCLUDING REMARKS AND RECOMMENDATIONS

This chapter is a summary of the conclusions that could be reached from the data discussed in the previous chapters. It is concluded with suggestions for future research on this same subject.

7.1 Conclusions

7.1.1 Method of activation

It was possible to achieve higher surface areas (as measured by the I_2 number) in the fluidised bed reactor when comparing the surface areas obtained in the rotary kiln to that of the fluidised bed reactor. A maximum I_2 number of 576 mg I_2 per gram carbon could be achieved in the reactor. This is, however, way below the standard required for the gold market.

As a hysteresis loop was obtained in some of the adsorption isotherms it can be concluded that the activated carbons contain mesopores. The increasing degree of hysteresis with increasing temperature suggests that the mesoporosity also increases with increasing temperature.

There was no significant difference in the pore size distributions between the two ways of activation. There was, however, in both cases a shift from micropore distributions towards mesopore distributions as the activation temperature increased.

A distinct maximum is observed that is higher for higher activation temperatures. Low temperature activation exhibits a rapid increase of the micropore volume up to approximately 6 hours HTt, possibly due to opening of restricted pores, whereas further burning off results only in minor changes in the micropore

volume. In the case of activation in the FB the mesopore development on the other hand is not as rapid as the micropore and exhibits a steady course of development. .

It can be concluded that low activation temperatures and treatment times lead to more microporous carbons than high activation temperatures.

As it was possible to manipulate the pore size distribution by varying the activation temperatures and conditions, this information can be fully utilised when a specific market sector is in mind for the use of the activated carbon.

7.1.2 Gold adsorption

It was observed that the Smartie coke activated carbon had a great affinity for gold cyanide. It compared well with the more preferred activated carbon currently in use in the gold mining industry.

Even though the rate of adsorption was faster for the Smartie coke and the equilibrium concentration was lower, the hardness of the Smartie coke needs to be evaluated under typical CIP conditions.

7.1.3 Water Purification

In the tests conducted it was showed that the Smartie coke activated carbon had the potential over a short period of time to remove impurities. There was however a de-selection of the organisms after a period of time. This could be attributed to the influence of certain functional groups.

7.2 Recommendations

It is suggested that the Smartie coke be activated not only with steam, but with other activating agents such as O₂ or CO₂ or combinations thereof. This should increase the surface area of the formed activated carbon and will then correlate more with the required surface area.

As there are different mixtures of Smartie coke, a study should be conducted on the effect of different ratios of Green MTP coke to waxy oil coke. This should increase or decrease the reactivity of the activated carbon.

In order to fully assess the utilisation of the activated carbon in the gold industry it will need to be tested under actual CIP plant conditions.

For the full use of the activated carbon in the water purification market it will be necessary to determine the functional groups present in the activated carbon and to what extent it has an influence on the adsorption of the dissolved organic components in the water.

References

- 1 Bansal R.C., Donnet J., Stoeckli H.F. [1988] in Active Carbon, (p vii)
Published by Marcel Dekker Inc., New York-Basel
- 2 Market analysis conducted by Chemical Marketing and Consulting
Services cc
- 3 Mattson, J. S., and Marx, H.B. Activated carbon. New York, Marcel Dekker,
1971
- 4 Yehaskel, A (ed.) Activated carbon-manufacture and regeneration. Park
Ridge (USA), Noyes Data Corporation, 1978
- 5 Smisek M., Cerny S. (eds.). Active Carbon-manufacture, properties and
applications. Elsevier, Amsterdam, 1970
- 6 Bansal R.C., Donnet J., Stoeckli H.F. [1988] in Active Carbon, (p 3)
Published by Marcel Dekker Inc., New York-Basel
- 7 Smisek M., Cerny S. Active Carbon, Elsevier, Amsterdam, 1970
- 8 Rodriguez-Reinoso F., Preparation and characterisation of activated
carbons (p 601) (1986)
- 9 Brunauer S. The adsorption of gases and vapours. Vol. 1, Physical
adsorption, Princeton University Press, Princeton, N.J. (1943)
- 10 Webb, P.A. and Orr, C. Analytical methods in fine particle technology.
Micromeritics Instrument Corporation, Norcross, USA. p. 56 – 57 (1997).
- 11 IUPAC Manual of Symbols and Terminology, Appendix 2, Pt. 1, Colloid
and Surface Chemistry, Pure and Appl. Chem. 31,578 (1972).
- 12 Brunauer S., Emmet P.H., and Teller E. J. Am. Chem. Soc. 60, 309 (1938)
- 13 Dubinin M.M [1966] in Chemistry and physics of carbon, Vol.2 (p51)
(Walker P.L., jr., ED.), Published by Marcel Dekker, New York,
- 14 Dubinin M.M Progress in Surface and Membrane Science, Vol 9
(Cadenhead D ed.) Academic Press, New York 1975
- 15 Dubinin M.M., Polystyanov E.F. [1966] Izv. Akad. Nauk. SSSR Ser. Khim
793

- 16 Dubinin M.M., Astakhov V.A. [1971] *Adv. Chem. Ser.* 102, 69
- 17 Webb, P.A. and Orr, C. *Analytical methods in fine particle technology.* Micromeritics Instrument Corporation, Norcross, USA. p. 81 – 85 (1997).
- 18 Webb, P.A. and Orr, C. *Analytical methods in fine particle technology.* Micromeritics Instrument Corporation, Norcross, USA. p. 63 (1997)
- 19 Davis, W.N., U.S. Patent 227, 963, 1880
- 20 Johnson, W.D., U.S. Patent 522, 260, 1894
- 21 Zadra, J.B., U.S. Bureau of Mines, Washington, D.C., R. I. No. 11672 (1950)
- 22 Zadra, J.B., Angel, A.K., and Heinen, H.J., U.S. Bureau of Mines, Washington, D.C., D.I. No. 4843 (1952)
- 23 Hall, K.B., *World Min.*, 27:44 (1974)
- 24 McDougall, G.J. and Hancock, R.D., Gold complexes and activated carbon. A literature review, *Gold Bul.*, 14 (1981) 138-153
- 25 Cho, E and Pitt, C.H., The adsorption of silver cyanide on activated charcoal, *Metall. Trans.*, 10B (1979) 159 – 164
- 26 McDougal, G.J., Hancock, R.D., Nicol, M.J., Wellington, O.L. and Copperwaite, R.G., The mechanism of the adsorption of gold cyanide on activated carbon, *J.S.Afr. Inst. Min. Metall.*, 80 (1980) 344 – 356
- 27 Tsuchida, N., Ruane, M. and Muir, D.M., Studies on the mechanism of gold adsorption on carbon, in: Haughton, L.F. (Ed.) *MINTEK 50, Proc. Int. Conf. On Recent Advances in Mineral Science and Technology*, Randburg, South Africa, Council for Mineral Technology, Vol.2 1984, pp 647 – 656
- 28 Davidson, R.J., 1974. The mechanism of gold adsorption on activated charcoal, *J S Afr. Inst. Min. Metall.*, 75 (4):67-76
- 29 McDougal, G.D., Adams M.D. and Hancock R.D. 1987 Models for the adsorption of aurocyanide onto activated carbon. Part 1: Solvent extraction of aurocyanide ion pairs by 1-pentanol, *Hydrometallurgy*, 18: 125-138
- 30 McDougal, G.D. and Flemming, C.A., 1987. Extraction of precious metals on activated carbon, in (Eds: M Streat and D Naden) *Ion exchange and*

- sorption processes in hydrometallurgy, Critical report on applied chemistry, 19: 56 –126, (John Wiley and Sons: Chichester UK).
- 31 Nicol, M.J., Flemming, C.A., and Paul, R.L. 1987. The chemistry of the extraction of gold, in (Ed: G.G. Stanley), The Extractive Metallurgy of Gold in South Africa, 2:870-877 (SAIMM: Johannesburg South Africa).
- 32 Adams, M.D., McDougall, G.J., and Hancock, R.D., 1987. Models for the adsorption of aurocyanide onto activated carbon. Part III: Comparison between the extraction of aurocyanide by activated carbon, polymeric adsorbents and 1-pentanol. Hydrometallurgy, 19:95-115
- 33 Adams, M.D. and Flemming, C.A., 1989. The mechanism of adsorption of aurocyanide onto activated carbon. Metall. Trans. B, 20B: 315-325
- 34 Adams, M.D. 1990 The mechanism of adsorption of aurocyanide onto activated carbon, 1. Relation between the effects of oxygen and ionic strength. Hydrometallurgy, 25:171-184
- 35 Dixon, S., Cho E., Pitt C.H. [1978] A.I. Ch. E Symposium Series 147 (173) 75
- 36 Tsuchida N.,Muir D.M. [1986] Metall. Trans. B 17B 523
- 37 Tsuchida N.,Muir D.M. [1986b] Metall. Trans. B 17B 529
- 38 Voges, S. 1996. The effect of the pore structure of activated carbon on gold adsorption
- 39 Van der Merwe, P.F., Van Deventer, J.S.J. [1988] Chem. Eng. Comm. 65 121
- 40 Smith, R. A., Proc. Roy. Soc (London) 12,424 1863
- 41 Rhead, T. F. E. and Wheler, R. V., J. Chem. Soc. 101, 846 (1912)
- 42 Rhead, T. F. E. and Wheler R. V., J. Chem. Soc. 103, 461 (1913)
- 43 Matson, J.S., Mark, H.B. Jr, and Weber, W.J. Jr., Anal. Chem, 41, 355 (1969)
- 44 Barton, S.S. and Harrison, B.H., Carbon 13,283 (1975)
- 45 Zawadski, J., Carbon 16, 491 (1978)
- 46 Ishizaki, C and Marti I., Surface oxide structures on a commercial activated carbon, Carbon 19, 411 (1980)

- 47 Fuerstenau M.C., Nebo C.O., Kelso J.R., Zaragoza M. (1987) *Mining Metals. Proc* **11** 177
- 48 McDougal G.J., Hancock R.D., Nicol M.J., Wellington O.L., Copperthwaite R.G., (1980) *J.S. Afr. Inst. Min. Metall.* **80(9)** 344
- 49 Van Deventer J.S.J. (1983) *Reagents in the Minerals Industry*. Institution of Mining and Metallurgy, London. Editor : M.J. Jones, pp 155-160
- 50 Ye, D.P., Agnew, J.B. and Zhang, D.K. *Fuel*, **77(11)**, 1209 (1998).
- 51 Sørensen, L.H., Saastamoinen, J. and Hustad, J.E. *Fuel*, **75(11)**, 1294 (1996).
- 52 Szekely, J. and Evans, J.W. *Chem. Eng. Sci.*, **26**, 1091 (1970).
- 53 Bhatia, S.K. and Perlmutter, D.D. *AIChE J.*, **26**, 379 (1980).
- 54 Lee, W.J. and Kim, S.D. *Fuel*, **74(9)**, 1387 (1995).
- 55 Hauman, D., Slabbert, R. and Prinsloo, F.F. Production of activated carbon in a fluidised bed reactor. SASTECH Report (1999).
- 56 Green, D.W., Hardy, Beri, and Vickburg. *Hydrocarbon Processing*. (1971) **50** (1) 105-108
- 57 Molina, A. and Mondragon, F. *Fuel*, **77(15)**, 1831 (1998).
- 58 M. Matsukata, E. Kikuchi and Y. Monta, *Fuel*, **71**, 319 (1992).